DEUTSCHES ELEKTRONEN-SYNCHROTRON DESY

DESY 86-032
March 1986

QCD, $\gamma\gamma$ AND HEAVY QUARK PHYSICS AT LEP

by

A. Ali
Deutsches Elektronen-Synchrotron DESY, Hamburg

ISSN 0418-9833

NOTKESTRASSE 85 · 2 HAMBURG 52

To be sure that your preprints are promptly included in the
HIGH ENERGY PHYSICS INDEX ,
send them to the following address (if possible by air mail) :

DESY
Bibliothek
Notkestrasse 85
2 Hamburg 52
Germany

DESY 86-032
March 1986

ISSN 0418-9833

QCD, $\gamma\gamma$ and Heavy Quark Physics at LEP *+

A. Ali

Deutsches Elektronen-Synchrotron DESY
D-2000 Hamburg 52, Federal Republic of Germany

ABSTRACT

This report gives a brief theoretical overview and summarizes the work done by the members of the working group on QCD, $\gamma\gamma$ and Heavy Quark Physics at LEP.

* In collaboration with and contribution from P. Aurenche (Annecy), A. Cordier (Orsay), G. Ekspong (Stockholm), S.D. Ellis (Washington, Seattle), D. Miller (Manchester), G. Rudolph (Innsbruck), R. Settles (MPI, München), W.J. Stirling (CERN) and K.H. Streng (München).

+ To be published in the proceedings of the LEP-Physics-Jamboree, CERN, Geneva, Switzerland

Individual Contributions

1. Testing the Gluon Self Coupling in $e^+e^- \rightarrow \gamma$, $Z^0 \rightarrow$ Four jets;
   G. Rudolph, University of Innsbruck, Austria

2. QCD Tests in Hadronic Decays of Orthotoponium;
   K.H. Streng, Sektion Physik, Universität München, Federal Republic of Germany

3. Measurements of the F_2 Photon Structure Function at LEP;
   A. Cordier, LAL-Orsay, France

4. Single Hadron Spectrum in two-photon Processes at LEP Energies;
   P. Aurenche et al., Annecy-le-Vieux, France

5. Vertex Detection at LEP;
   R. Settles, Max-Planck-Institut für Physik und Astrophysik, München, Federal Republic of Germany

6. Heavy Quark Physics at LEP;
   A. Ali, DESY, Federal Republic of Germany

E R R A T U M

QCD, $\gamma\gamma$ and Heavy Quark Physics at LEP

A. Ali

DESY Report DESY 86-032 (1986)
(also published in CERN Yellow Report 86-02 Vol.2 (1986) p.81)

i) The second reference in Ref. 18) quoted as M. Glück and E. Reya, Phys.Rev. D20, 2740 (1983) and DO-TH-84/12 (1984), should be replaced by the following reference:

M. Drees, M. Glück and E. Reya, Phys.Rev. D30, 2316 (1984).

ii) The reference in the Figure Captions for Figs. (28) and (29) should be read as :

(from Drees et al., in Ref. 18)).

The above-mentioned errors are very much regretted.

Introduction

Electron positron annihilation physics is one of the main fields where knowledge of Quantum Chromodynamics, QCD, has been successfully applied in the studies of final states formed as a result of direct annihilation $e^+e^- \rightarrow \gamma \rightarrow X$. True, most applications of QCD in e^+e^- physics are restricted to the level of perturbation theory and in many cases, the non-perturbative contributions have either to be modelled or extracted from the data. Yet, the successes of perturbation theory in e^+e^- annihilation are convincing and the QCD tests have reached a precision level which is both quantitative and impressive [1]. To quote a few examples, one could cite the prediction of the total hadronic cross-section [2], the existence of quark jets first proven in QCD by Sterman and Weinberg [3], the prediction [4] and discovery [5] of gluon jets in e^+e^- annihilation, tests of the quark and gluon spins [6], calculations of jets in $O(\alpha_s)^2$ [7] and measurements of the effective coupling constant [8], $\alpha_s(Q^2)$. In addition to the continuum e^+e^- annihilation physics, there are two more areas in e^+e^- physics, where rapid progress has been made in the past both experimentally and theoretically. The first area concerns the heavy-Onia physics studied via J/ψ, η_c, χ states at SPEAR and DORIS [9] and Υ, χ_b,... systems at CESR and DORIS [10]. The second area concerns the measurements of the two-photon processes $e^+e^- \rightarrow e^+e^-x$, [11] notably the first measurements of the photon structure function, F_2^γ at PEP and PETRA [12]. The sum total of this experience constitutes an integral part of the impecable evidence for QCD as the theory of strong interactions in high energy physics.

Since the field of QCD has matured mainly though not exclusively through applications in e^+e^- annihilation, novel tests and fancy ideas are not easy to find. There is, however, one quantitative difference between the physics at PEP and PETRA on one hand and the LEP Physics on the other, which may reveal some not so well studied aspects of QCD. The expected vector meson resonances at LEP, namely Z^0 and the toponium states $\theta, \theta', \ldots$ etc., have large masses. This would allow kinematic reconstruction of multijet states in particular 4-jet states in the decays $Z^0 \rightarrow 4$ jets, [13] and $\theta, \theta', \ldots \rightarrow 4$ jets [14]. In addition, the rates at Z^0, with the estimated cross-section $\sigma(Z^0) \simeq 30$ nb, are expected to be large, yielding several million Z^0 events in a typical year. Thus, study of the 4-jet final states at LEP is an obvious field

where detailed tests of QCD would be made. Since in e^+e^- annihilation, the full non-abelian gauge structure of QCD is unfurled only in (at least) 4-jet final states, experiments at LEP are expected to provide new quantitative tests of this aspect of QCD. Because of this we have concentrated on the final states $Z^0 \rightarrow 4$ jets and $\theta \rightarrow 4$ jets, γ + 3 jets with the view of testing the non-abelian nature of QCD. We shall give a resumé of this study in the next section (i.e. section 2), where we also review some salient features of hadronic final states at LEP energies in the context of QCD.

In section 3 we review the subject of $\gamma\gamma$ physics at LEP [15]. Here we have studied in detail two aspects namely, the quality of the photon structure function F_2^γ measurements at LEP [16] and the large-p_T production of hadrons in the process $\gamma\gamma \rightarrow hX$. [17] For both of these points, estimates and counting rates are presented calculated in perturbative QCD as well as in vector dominance models. The quality of 2γ physics at LEP would depend strongly on the forward detection capability and this differs from experiment to experiment. However, generally speaking a much larger Q^2 rangle will be available at LEP compared to PEP and PETRA experiments. Since F_2 rises as $\log(Q^2/\Lambda^2)$ in QCD, it would be possible to see this rise and measure F_2^γ for a larger value of the invariant mass, W and the photon virtuality Q^2. The photon structure functions at LEP will be sensitive to heavy quark flavours, including the bottom quark. However, the virtuality Q^2 at LEP is not large enough to feel the $t\bar{t}$ threshold in F_2^γ or F_L^γ (assuming $m_t \simeq 40$ Gev). By the same token neither F_2^γ nor the longitudinal structure function F_L^γ could feel the presence of supersymmetric particles [18] through the production $\gamma\gamma^* \rightarrow \tilde{q}\bar{\tilde{q}}$, $\tilde{g}\tilde{q}$, again assuming $m_{\tilde{q}} \gtrsim 40$ GeV, the limit suggested by the recent UA1 data [19]. Thus, LEP experiments will be able to measure the QCD contribution to F_2^γ and F_L^γ in an almost threshold free background.

In analogy with the annihilation process $e^+e^- \rightarrow \gamma$, $Z \rightarrow hX$, the QCD corrections will lead to p_T broadening of hadrons in the process $\gamma\gamma \rightarrow hX$. Part of this cross-section will result in two jet events emanating from the process $\gamma\gamma \rightarrow q\bar{q}$. Again, the experiments at LEP will have quantitative advantage over those at PEP and PETRA, where both the large p_T^h tail as well as jets in 2γ processes are dominated by hadronic wave function effects.

The other interest in $\gamma\gamma$ physics lies in its capability of singly producing neutral, even charge conjugate states. In the past this has led to the production of π^0, η, η', δ, f, A_2 and f' and measurement of their two-photon widths [11]. The most sought after and eagerly awaited even charge conjugation particle is the Higgs boson. The problem here lies in the width $\Gamma(H^0 \to 2\gamma)$ which in the standard model is expected to be $\lesssim 2$ eV for $m_{H^0} \lesssim 5$ GeV. [20]. This, unfortunately is too small a width to be seen in $\gamma\gamma$ experiments. The same comments apply to the searches of neutral technipions. For more massive Higgs, $m_H > 10$ GeV, the $\gamma\gamma$ luminosity $\mathcal{L}(m_H^2/s)$ would become too small also at LEP, and this then allows only for a restricted Higgs search in $\gamma\gamma$ processes.

Perhaps, it should be possible to search for glueballs in the process $\gamma\gamma \to X$ with some luck. The widths of the glueballs are not yet reliably calculable. Present estimates of scalar glueballs in the mass range 0.5 GeV vary between 1 eV [21] and several hundred eV [22]. Again a 1 eV width appears to be at the outer verge of experimental feasibility. The discovery potential of $\gamma\gamma$ physics at LEP in terms of exotic particle searches is not particularly high. This becomes clear if one compares the $\gamma\gamma$ luminosity at LEP with the corresponding gg luminosity at the present CERN $\bar{p}p$ collider [23]. In view of this we have decided to confine ourselves to the discussion of standard physics problems in $\gamma\gamma$ physics at LEP.

The third part of this report covers some aspects of heavy quark physics at LEP [24]. Since the branching ratio for $Z^0 \to b\bar{b}$ is expected to be ~ 15 % in the standard model, Z^0 decays would provide $\mathcal{O}(10^6)$ bottom hadrons in a typical year. Thus, LEP would be a powerful bottom hadron factory and we expect a very fruitful research programme studying bottom hadron decay properties. In addition to enjoying the benefit of a very intense bottom hadron source, the experiments at LEP and SLC are expected to have vastly improved vertex detection facilities [25]. A good part of the report on heavy quark physics is therefore concentrated on bottom quark physics. The issues that we have addressed in this section concern the potential of LEP in determining the strength of the $b \to u$ transitions, the strength of the effective $|\Delta B| = 2$, $\Delta Q = 0$ transitions leading to B-$\bar{B}$ oscillations, and the possibility of observing

CP violations in the bottom hadron sector.

The other interest in Z^0 decays lies in the decays $Z^0 \to t\bar{t}$, if they are kinematically available. More massive top quarks would otherwise be produced in e^+e^- continuum though at a much reduced rate. The first point to confirm here would be to check if the top quark indeed belongs to a b-quark doublet with canonical couplings and properties. [26] The other points of interest are the relative strengths of the transitions $t \to b$, $t \to s$ and $t \to d$. We have discussed ways to measure these transitions. In addition to this, the large mass for the top quark introduces new aspects concerning the top quark polarization effects [27], which have measurable effects on a large number of production and decay distributions. We have reviewed some interesting aspects of top quark polarization effects, relevant for experiments at LEP.

The general format of this report is as follows. We review in this article salient features of our group study together with some relevant background material. The individual reports, which go in depth, on specific issues are being published separately in these proceedings.

2. QCD in e^+e^- annihilation physics

2.1 Total hadronic cross-sections in $e^+e^- \to$ hadrons

We shall review in this section some aspects of QCD, already well known from e^+e^- physics at PEP and PETRA and lower energies, and some others, mainly involving 4-jets, which we expect to be quantitatively studied at LEP energies. We start with the measurements of the inclusive hadronic cross-section in the electromagnetic production $e^+e^- \to \gamma \to X$. The changes that one needs to include in the complete electroweak production for $\sigma(e^+e^- \to \gamma, Z \to X)$ have been discussed in detail in an accompanying report [24], and hence will not be repeated here.

The total hadronic cross-section in the quark-parton model is usually expressed in terms of the ratio $R \equiv \sigma(e^+e^- \to \gamma \to \text{hadrons})/\sigma(e^+e^- \to \gamma \to \mu^+\mu^-)$ (the subscript on R signifies the order in α_s).

$$R_o = 3 \sum_i Q_i^2 \phi_i \qquad (2.1)$$

where Q_i are the electric charges of the quarks and ϕ_i is a phase-space factor

$$\phi_i = \beta_i^2 \left(\frac{3-\beta_i^2}{2}\right) \xrightarrow[\beta_i = 1]{} 1 \qquad (2.2)$$

and β_i is the quark velocity in the e^+e^- rest frame, $\beta_i = (1-4m_i^2/Q^2)^{1/2}$ with $Q^2 = 4E^2_{beam}$. In $O(\alpha_s)$, the constant R has the following value [28]

$$R_1 = R_0\left(1 + 4/3\ \alpha_s^{(1)}(Q^2) f(\beta_i)\right)$$
$$f(\beta_i) = \frac{\pi}{2\beta_i} - \left(\frac{3+\beta_i}{4}\right)\left(\frac{\pi}{2} - \frac{3}{4\pi}\right) \qquad (2.3)$$
$$\xrightarrow[\beta_i = 1]{} 3/4$$

Hence in this limit

$$R_1 = R_0\left(1 + \frac{\alpha_s^{(1)}(Q^2)}{\pi}\right) \qquad (2.4)$$

with

$$\alpha_s^{(1)}(Q^2) = \frac{12\pi}{(33-2n_f)\ln(Q^2/\Lambda^2)} \qquad (2.5)$$

Again the changes that occur in going over from electromagnetic to electroweak description are detailed in ref. (24). We only remark that the expression (2.4) for the massless quarks also holds for the process $e^+e^- \to \gamma$, $Z \to$ hadrons, with appropriate value for R_0 obtaining in the standard electroweak model. Since at LEP energies, $\beta_i \simeq 1$ for u,d,s,c and b quarks, eq. (2.4) is an adequate description of σ_{tot} ($n_f = 5$) in $O(\alpha_s)$. The velocity dependent corrections are quite important for the top quark. This case is discussed separately in ref. (24) as well as by the toponium study group [29]. In $O(\alpha_s)^2$, the ratio R has the value [30]

$$R_2 = R_0\left(1 + \frac{\alpha_s(Q^2)}{\pi} + C_2\left(\frac{\alpha_s(Q^2)}{\pi}\right)^2\right) \qquad (2.6)$$

where the coefficient c_2 depends on the renormalization scheme and in the popular $\overline{MS}$ scheme [31] has the value

$$c_2 = 1.98 - 0.115\ n_f = 1.41 \text{ for } n_f = 5 \qquad (2.7)$$

For $\alpha_s(Q^2) = 0.1$, as expected at LEP energies, the $O(\alpha_s)^2$ term in R_2 contributes at the level of 1.4 p.p.m. and hence is completely negligible. The important point to remember is that the function $\alpha_s(Q^2)$ is defined using two-term beta function and has the form

$$\alpha_s(Q^2) = \alpha_s^{(1)}(Q^2)\left(1 - \frac{\alpha_s^{(1)}(Q^2)}{\pi}\frac{\tilde{\beta}_1}{\tilde{\beta}_2}\ln\ln(Q^2/\Lambda^2)\right) \qquad (2.8)$$

where

$$\tilde{\beta}_1 = (33 - 2n_f)/3$$
$$\tilde{\beta}_2 = (306 - 38n_f)/3 \qquad (2.9)$$

Thus $\alpha_s(Q^2) < \alpha_s^{(1)}(Q^2)$ for the same value of Λ. Again eqs.(2.6)-(2.9) are valid for the complete electroweak case $e^+e^- \to \gamma$, $Z \to$ hadrons, in the limit $\beta_i = 1$. The $O(\alpha_s^2)$ corrections in R for the massive quark case have not yet been calculated. In view of the large $O(\alpha_s)$ corrections in R for the top quark case, one wonders how convergent the series is in $O(\alpha_s)^2$. A clue to the importance of $R_2(t\bar{t})$ may come from an experimental comparison of $R_2(t\bar{t})$ and $R_2(n_f = 5)$ in terms of the QCD parameter, $\Lambda_{\overline{MS}}$.

The power corrections to R have been calculated by the ITEP group. [32] The corrections to the I=1 part of R in the ITEP sum rule approach can be expressed as

$$\int_{4m_\pi^2}^{\infty} e^{-s/M^2} R^{I=1}(s)\,ds$$
$$= \frac{3}{2}\Big(1 + \frac{\alpha_s(M^2)}{\pi} + C_2\left(\frac{\alpha_s(M^2)}{\pi}\right)^2$$
$$+ \frac{\pi^2}{3M^4}\langle 0|\frac{\alpha_s(M^2)}{\pi} G^a_{\mu\nu} G^a_{\mu\nu}|0\rangle$$
$$- \frac{448\pi^3}{81M^6}|\langle 0|\bar{q}q|0\rangle|^2 + \cdots\Big) \qquad (2.10)$$

where $G^a_{\mu\nu}$ is the QCD field-strength tensor. At LEP energies, with $Q^2 \simeq s \gg m_Z^2$, the ITEP mass parameter M^2 should be chosen large $M^2 \sim O(Q^2)$. Thus at LEP energies the power correction terms $\langle 0|G^a_{\mu\nu} G^a_{\mu\nu}|0\rangle/Q^4$ and $\langle 0|\bar{q}q|0\rangle/Q^4$ are completely negligible and we shall ignore them.

Of course, all of what we have said so far applies verbatim for the measurements of R at PEP and PETRA energies. With $O(10^5)$ hadronic events available in a typical experiment at PEP and roughly a factor 2 less at PETRA, statistics is certainly not the obstacle in determining $\alpha_s(Q^2)$ from R. We show in table 1 a summary of the present measurements of R [33] for 29 GeV $\lesssim \sqrt{s} \lesssim$ 36.7 GeV at PEP and PETRA together with the determination of α_s. It is easy to see that the errors are dominated

Experiment	$\sqrt{s}$ (GeV)	$R \pm \Delta R^{stat.} \pm \Delta R^{syst.}$	$\alpha_s \pm \Delta\alpha_s^{stat.} \pm \Delta\alpha_s^{syst.}$
JADE	30-36.7	$3.99^{\pm}0.04^{\pm}0.1$	$0.20^{\pm}0.03^{\pm}0.08$
MAC	29.0	$3.87^{\pm}0.10^{\pm}0.1$	$0.15^{\pm}0.06^{\pm}0.08$
MARK J	30.0-36.7	$3.95^{\pm}0.05^{\pm}0.22$	$0.18^{\pm}0.03^{\pm}0.15$
MARK II	29.0	$3.90^{\pm}0.05^{\pm}0.25$	$0.17^{\pm}0.03^{\pm}0.17$
TASSO	30-36.7	$4.05^{\pm}0.05^{\pm}0.19$	$0.24^{\pm}0.04^{\pm}0.13$

Table 1. A summary of R measurements at PEP and PETRA and α_s values deduced from the R values (from ref. (33)).

by systematics, a non-negligible fraction of which is due to the lack of $O(\alpha)^4$ electroweak radiative corrections. The $O(\alpha)^3$ corrections to R are numerically very important also at LEP [34]. Hence in all likelihood $O(\alpha)^4$ contributions will also have non-negligible effect at the level of 1-2 % that we are discussing. Assuming that these corrections would be available before the turnon of LEP, the important question would still be to estimate the intrinsic limitations on ΔR in a typical experiment at LEP due to measurement errors. The JADE and MAC collaborations at PETRA and PEP, respectively, have claimed a systematic error $\Delta R/R = \pm$ 2.5 %. Though this is not the place to give an objective critique of such error estimates, it is worthwhile to start seriously thinking about systematic errors in the measurements of R at LEP and SLC energies. An error $\Delta R/R = \pm$ 1 % should certainly be the goal if $\alpha_s(Q^2)$ determination at $\pm$ 20 % is to be achieved from R measurements

at LEP.

2.2 Charge asymmetries in $e^+e^- \to \gamma$, $Z \to$ hadrons

In the quark parton model, a forward backward quark charge asymmetry is expected due to the vector-axial vector interference in the process $e^+e^- \to \gamma$, $Z \to l^+l^-$, hadrons. [35] The asymmetries in $e^+e^- \to \gamma, Z \to l^+l^-$ (l = e, μ,) have been measured at PETRA and PEP and are found to be in reasonable agreement with the expectations in the standard model [36]. The measurements of the charge asymmetry in $e^+e^- \to q\bar{q}$ have also been reported at PETRA and PEP, though these measurements are still in their preliminary stage. [37] Of course, experimentally, such measurements require the ability to distinguish between the quarks and anti-quarks. Luckily, the semileptonic decays $c \to l^+x$, $b \to l^-x$ etc. do provide such distinctions. The improved ability of LEP detectors in terms of vertex reconstruction of the charmed and bottom hadrons would provide an additional quark/anti-quark distinction. Crucial in this context is the point that in $e^+e^- \to \gamma$, $Z \to QX$, heavy flavour (c,b,t) production takes place dominantly only at the electroweak vertex $\gamma, Z \to Q\bar{Q}$. The $O(\alpha_s)^2$ and higher order processes do lead, in principle, to final states of the type $e^+e^- \to q\bar{q}g \to Q\bar{Q}$ and $e^+e^- \to Q\bar{Q}Q\bar{Q}$, which in general reduce the asymmetry. [38] However, both data at PETRA/PEP and explicit QCD calculations lead to a very small production (at the level of few parts in 10^3) of multiple heavy quark final states. [39]

We have discussed in a companion report the forward-backward asymmetry, A^q_{FB}, in the quark-parton model as well as $O(\alpha_s)$ QCD and quark mass corrections to A^q_{FB} defined as

$$A^q_{FB} \equiv \frac{\left[\int_0^1 \frac{d\sigma}{d\cos\theta}(e^+e^- \to q\bar{q}X) - \int_{-1}^0 \frac{d\sigma}{d\cos\theta}(e^+e^- \to q\bar{q}X)\right] d\cos\theta}{\left[\int_0^1 \frac{d\sigma}{d\cos\theta}(e^+e^- \to q\bar{q}X) + \int_{-1}^0 \frac{d\sigma}{d\cos\theta}(e^+e^- \to q\bar{q}X)\right] d\cos\theta} \qquad (2.11)$$

Again, the QCD and mass corrections are important for the top-quark asymmetry measurements at LEP energies. The $O(\alpha_s)^2$ corrections to A^q_{FB} have so far been calculated only partially. In particular, the $O(\alpha_s)^2$ virtual corrections to the terms odd in $\cos\theta$ in the process

$e^+e^- \to \gamma$, $Z \to q\bar{q}$ leading to A_{FB}^q are not yet available.

With the emergence of well-defined quark and gluon jets in e^+e^- annihilation, a lot of experience has been gained in working with jets. [40] In particular, it is possible to select kinematic configurations in an experiment which project out final states with a definite number of jets. Thus, for example, using a prescription due to Sterman and Weinberg [3] it is possible to define an n-jet cross-section $\sigma_n(\varepsilon,\delta)$ where $\varepsilon = \min(E_i/E_{beam})$ and $\delta = \min(\theta_{ij})$, with E_i and θ_{ij} being the energies of and angles between quarks and gluon jets. One could also select final states which eliminate two- and three-jet configurations. This, for example can be achieved by cuts on the variable thrust [41], defined as

$$T = \max. \frac{\sum_i |\vec{P}_{iL}|}{\sum_i |\vec{P}_i|} \qquad (2.12)$$

with the boundary $1 \geqslant T \geqslant 0.5$ or on the variable acoplanarity [42], defined as

$$A = 4 \min. \left(\frac{\sum_i |\vec{P}_{iT,out}|}{\sum_i |\vec{P}_i|} \right)^2 \qquad (2.13)$$

with the boundary $2/3 \geqslant A \geqslant 0$. Then kinematic configuration with $1-T > 0$ would eliminate 2-jet events and $A > 0$ would eliminate 3-jet events. The advantage of ordering the final states in jets with definite multiplicity is theoretical expediency. For example, calculating the distribution $d\sigma/dT(T < 1)$ liberates one from calculating the contributions due to $e^+e^- \to \gamma$, $Z \to q\bar{q}$ and virtual corrections. Similarly, the distribution $d\sigma/dA(A > 0)$ receives contributions from the 4-jet processes $e^+e^- \to q\bar{q}gg$, $q\bar{q}q\bar{q}$ in leading order. QCD predicts [43] the existence (i.e. finiteness) of cross-sections $\sigma_n(\varepsilon,\delta)$ with a definite jet multiplicity and of distributions in linear variables, like thrust, energy-energy correlations and acoplanarity. Not only that these semi-inclusive cross-sections are finite but in measurements which distinguish between quarks and anti-quarks, one can define a large number of quark-charge forward-backward or azimuthal angle asymmetries, which are all calculable in QCD and experimentally measurable in high statistics experiments.

To illustrate these remarks, we shall review the charge dependent angular asymmetries predicted by QCD for three and four jet events. One can define (i) the forward-backward asymmetry of the thrust axis with respect to the electron momentum vector in 3-jet events. The kinematics for $e^+e^- \to q\bar{q}g$ is shown in fig. (1), and the polar angle asymmetry of the thrust axis is then

$$A_\theta \equiv \frac{\left[\int_{\theta \leq \pi/2} d\sigma/dx_q\, dx_{\bar{q}}\, d\cos\theta - \int_{\theta \geqslant \pi/2} \right] d\cos\theta}{\left[\int_{\theta \leq \pi/2} d\sigma/dx_q\, dx_{\bar{q}}\, d\cos\theta + \int_{\theta \geqslant \pi/2} \right] d\cos\theta} \qquad (2.14)$$

and (ii) an azimuthal forward-backward asymmetry with respect to the component of the e^+ momentum orthogonal to the thrust axis

$$A_\chi \equiv \frac{\left[\int_{|\chi| \leq \pi/2} d\sigma/dx_q\, dx_{\bar{q}}\, d\cos\theta\, d\chi - \int_{|\pi-\chi| \leq \pi/2} \right] d\chi(\theta=\pi/2)}{\left[\int_{|\chi| \leq \pi/2} d\sigma/dx_q\, dx_{\bar{q}}\, d\cos\theta\, d\chi + \int_{|\pi-\chi| \leq \pi/2} \right] d\chi(\theta=\pi/2)} \qquad (2.15)$$

The decomposition for the differential cross section $d\sigma/dx_q\, dx_{\bar{q}}\, d\cos\theta\, d\chi$ with $x_i = 2E_i/\sqrt{s}$ is given in Appendix A. The explicit expressions for the structure functions were derived in $O(\alpha_s)$ in ref. (44). These asymmetries are shown in fig. (2) for the u quark (= c quark) and d quark (≃ b quark) as a function of $\sqrt{s}$ with the cut-off T = 0.7, 0.8 and 0.9. All of these asymmetries are quite small near the Z^0 pole for unpolarized beams but are measurable below and above m_Z. However, if the electron and/or positron are longitudinally polarized then the electroweak coupling constant factor in A_θ and A_χ gets enhanced. The explicit dependence of them on the longitudinal polarization of the electron and positron is given in the appendix of ref. (46).

While on the subject of oriented 3-jet events and the corresponding asymmetries, we refer here to the extensive work done in refs. (45), in calculating all the $O(\alpha_s)^2$ corrections to the complete set of 4 linearly independent parity conserving and 2 parity

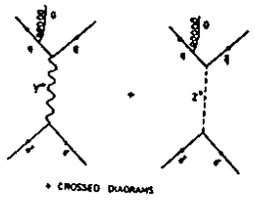

Fig. 1(a): $q\bar{q}G$ production in e^+e^- collisions via electromagnetic and weak interactions

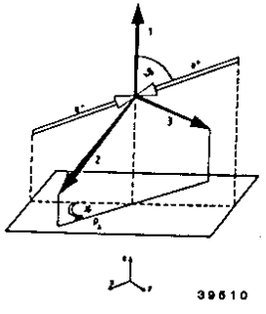

Fig. 1(b): Three-jet event in the CM frame. The thrust axis is the z axis (momentum 1). The $q,\bar{q}$ and G momenta define the (χ,z) plane. χ is defined by the antiquark (quark) if the thrust axis is given by the quark (antiquark) momentum; if the gluon is the most energetic particle, χ is marked by the quark. The angles θ and χ vary between $0 \leq \theta \leq \pi$, $0 \leq \chi \leq 2\pi$.

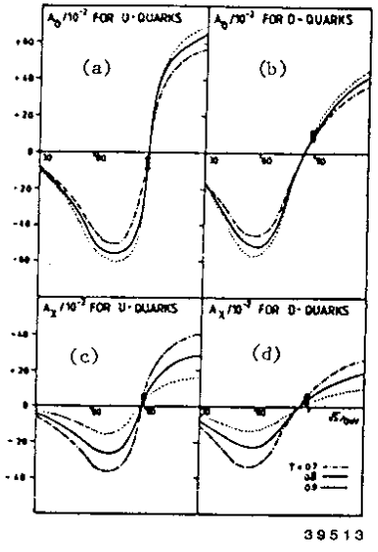

Fig. 2: Angular asymmetries of u- and d-jet distributions as functions of the CM energy for three thrust values; (a,b) forward-backward asymmetry of the thrust axis, defined by the q jet, with respect to e^- momentum; (c,d) azimuthal forward-backward asymmetry of the corresponding $\bar{q}$ jet.

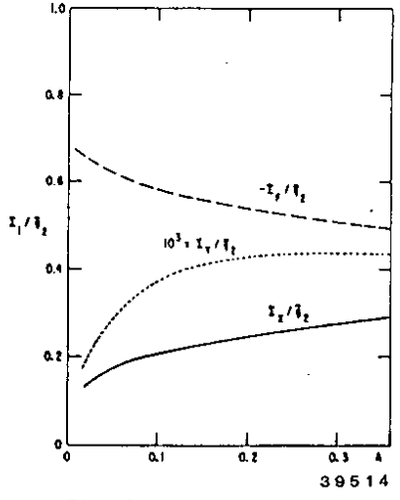

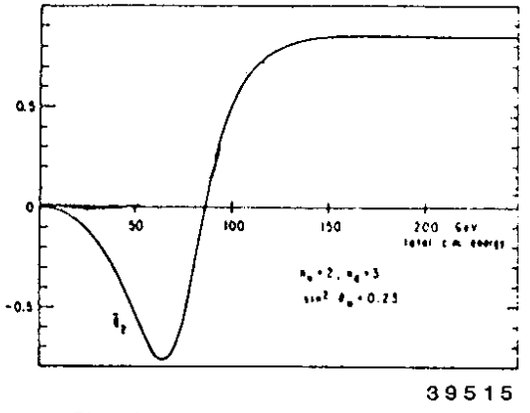

Fig. 4: Normalized flavor-dependent functions $\tilde{g}_2 = g_2/g_1$

Fig. 3: QCD factors of the asymmetries of the acoplanarity distributions as defined in Eq. (2.29)

violating structure functions shown in the decomposition of $e^+e^- \to \gamma, Z \to q\bar{q}g$ final states in the Appendix. This rather elaborate higher order QCD machinery will find extensive use at LEP and SLC energies, where the beam polarization and the huge statistics will enable to disentangle most of the structure functions. True, these calculations have been done for the massless quark case, but this is certainly a good approximation for u,d,s,c and b quarks produced in Z decays or otherwise at LEP energies.

The hadronic (quark) charge asymmetries for the 4-jet case in the process $e^+e^- \to q\bar{q}gg$, $q\bar{q}q\bar{q}$ have also been studied in literature. [46] We give here a brief account of the four jet kinematics first and then discuss the corresponding quark charge asymmetries. Defining the differential cross-section for four parton final state in e^+e^- annihilation as

$$d\sigma = (4\pi\alpha)^2 (4\pi\alpha_s(Q^2))^2 \times (2Q^6)^{-1} |M|^2 N_{stat.}^{-1} \, d\Omega^{(4)} \qquad (2.16)$$

where $N_{stat} = 2,4$ for the $q\bar{q}gg$ and $q\bar{q}q\bar{q}$ case and the Lorentz-invariant amplitudes $|M|^2$ for the most general case $e^+e^- \to \gamma$, $Z \to 4$ partons with $m_{parton} = 0$ and arbitrary lepton polarizations have been given in ref. (46). The invariant phase space $d\Omega^{(4)}$ can be expressed as

$$d\Omega^{(4)} = (2\pi)^4 \delta^4\left(q - \sum_i p_i\right) \prod_{i=1}^{4} d^3p_i/(2E_i 2\pi^3) \tag{2.17}$$

In discussing the charge asymmetries it is convenient to define two differently oriented center-of-mass frame S_L, for the initial leptons, and S_H, for the final hadrons. (47) The relative orientation of S_L and S_H is determined by the three Euler angles (θ, ϕ, ψ), which can be defined in the sense of Goldstein. (48) Then specifically, we could choose S_H such that the $\vec{p}_i(x,y,z)$ components are

$$\begin{aligned}
\vec{p}_1 &= E_1(0,0,1) \\
\vec{p}_2 &= E_2(\sin\beta,\ 0,\ \cos\beta) \\
\vec{p}_3 &= E_3(\sin\gamma\cos\alpha,\ \sin\gamma\sin\alpha,\ \cos\gamma) \\
\vec{p}_4 &= -\vec{p}_1 - \vec{p}_2 - \vec{p}_3
\end{aligned} \tag{2.18}$$

Then, in S_H, the components of the positron 3-momenta p^+ are

$$\vec{p}^{\,+}\big|_{SH} = |\vec{p}^{\,+}|\,(\sin\theta\sin\psi,\ \sin\theta\cos\psi,\ \cos\theta) \tag{2.19}$$

The phase space integral $d\Omega^{(4)}$ can be expressed as

$$d\Omega^{(4)} = 1/8\ Q^4(2\pi)^{-8}\, d\cos\theta\, d\psi\, d\phi\, dI^{(5)} \tag{2.20}$$

where

$$dI^{(5)} = Q^{-10} A_N^{-1/2}\, \theta(A_N)\, dz\, dx\, dy\, dt\, du\, ds \times \delta(1/2Q^2 - z - x - y - t - u - s) \tag{2.21}$$

$A_N = 0$ gives the boundary of the physical region and the quantity A_N itself is defined via the relation

$$Q^8 A_N = 4xuyt - (zs - xu - yt) \tag{2.22}$$

The variables $z, x, y, \ldots$ are defined in terms of the scalar product $p_i\, p_j$ and have the values

$$(z, x, y, t, u, s) = (p_1\,p_2, p_1\,p_3, p_1\,p_4, p_2\,p_3, p_2\,p_4, p_3\,p_4) \tag{2.23}$$

The phase space is not completely specified by eqs. (2.20) and (2.21) in the presence of pseudoscalar quantities. In that case eq. (2.20) is modified to

$$d\Omega^{(4)} = 1/16\ Q^4(2\pi)^{-8}\, d\cos\theta\, d\phi\, d\psi\, dI^{(5)} \sum_{sign = \pm} \tag{2.24}$$

where the sign is that of the pseudoscalar quantity

$$\tilde{e} = Q^{-4}\,\epsilon_{\mu\nu\lambda\rho}\, p_1^{\mu} p_2^{\nu} p_3^{\lambda} p_4^{\rho} \tag{2.25}$$

Normalizing in terms of the point-like cross-section for $e^+e^- \longrightarrow \mu^+\mu^-$, one has

$$1/\sigma_{\mu\mu}\,(2\pi\, d\sigma)/d\cos\theta\, d\phi\, d\psi = 3/32\pi^2 \left(\alpha_s(Q^2)/\pi\right)^2 |M|^2 N_{stat.}^{-1}\, dI^{(5)} \tag{2.26}$$

If the relative orientation of the lepton to the hadrons are integrated, then the averaged four-jet cross-section is obtained from

$$\langle d\sigma \rangle = \int d\sigma/d\cos\theta\, d\phi\, d\psi\ d\cos\theta\, d\phi\, d\psi \tag{2.27}$$

The purely electromagnetic case was first derived in ref. (39), with the result

$$\langle d\sigma^{\gamma\gamma} \rangle/\sigma_{\mu\mu} = -1/8\pi \sum_i Q_i^2 \left(\alpha_s(Q^2)/\pi\right)^2 Q^2 H_{\mu}^{\ \mu} N_{stat.}^{-1} \times dI^{(5)} \tag{2.28}$$

where $H_{\mu\mu}$ is given in the Appendix of refs. (39) and (66) for the

$e^+e^- \to q\bar{q}gg$ and $e^+e^- \to q\bar{q}q\bar{q}$ cases. We shall come back to a discussion of σ_{4jet} later but would like to define first the quark charge asymmetries in the four-jet case. One can define them as follows [45]

$$\left.\begin{matrix} d\Sigma^F \\ d\Sigma^X \\ d\Sigma^Y \end{matrix}\right\} = 1/\sigma_{\mu\mu} \int d\cos\theta\, d\psi\, d\phi \left(d\sigma/d\cos\theta\, d\psi\, d\phi\right) \times \left\{\begin{matrix} \epsilon(\cos\theta) \\ \epsilon(\sin\psi) \\ \epsilon(\cos\psi) \end{matrix}\right. \qquad (2.29)$$

with $\epsilon(x) = \pm 1$ for $x \gtrless 0$. In fig. (3) we show the normalized differential distributions [45] $1/\tilde{\sigma}_2 (d\Sigma^F/dA, d\Sigma^X/dA, d\tilde{\Sigma}^Y/dA)$ where $d\tilde{\Sigma}^Y$ means that a factor $\theta(E_1-E_2)\theta(E_3-E_4)\theta(\tilde{e})$ has been introduced for $d\Sigma^Y$. The normalized coupling constant $g_2(Q^2)$ is defined as

$$\tilde{g}_2(Q^2) = g_2(Q^2)/g_1(Q^2) \qquad (2.30)$$

and $\tilde{g}_2(Q^2)$ is shown in fig. (4). We note the tiny $\cos\psi$ asymmetry $d\tilde{\Sigma}^Y$. However, the asymmetry $d\Sigma^F$ (which is the analogue of A_{FB}^q for two-jet events) and $d\Sigma^X$ are large and hence measurable. Note that the precise value of Σ^F and Σ^X does not depend sensitively on the presence or absence of the non-abelian coupling.

None of the quark charge asymmetries A_θ, A_χ, Σ^F and Σ^X have been measured yet at the PETRA and PEP region. This is mainly because of the paucity of 3- and 4-jet events with well-identified quark and antiquark jets with well defined charges. These asymmetries play the same role for 3- and 4-jet events as the forward backward asymmetry for the 2-jet events and their measurements will constitute yet another quantitative test of the standard model and QCD.

2.3 Jets in e^+e^- annihilation

Hadronic jets were discovered in e^+e^- annihilation. The first experimental evidence for the dominance of two-jet final states in e^+e^- annihilation was presented by the SLAC-LBL collaboration at SLAC . Three jet events were first observed in experiments at PETRA in e^+e^- continuum [5] and in Υ decays at DORIS . Preliminary evidence of four-jet final states has also been reported at PETRA [49], though a detailed quantitative study of the 4-jet-properties is not yet available at PETRA and

probably would be forthcoming in experiments at LEP.

Theoretically, the existence of jets in QCD was first proven by Sterman and Weinberg [3] in the process $e^+e^- \to$ 2 jets, who calculated the cross-section $\sigma_{2jet}(\varepsilon,\delta)$ for two opposite cones of half angular size δ having all but a fraction ε of the total e^+e^- energy, obtaining (σ^0 is the lowest order cross-section for $e^+e^- \to q\bar{q}$)

$$\sigma^{2jet}(\varepsilon,\delta) = \sigma^0 \left[1 + 2\alpha_s(Q^2)/3\pi \times \left\{-4\ln\varepsilon\ln\delta^2 - 3\ln\delta^2 - 2\pi^2/3 + 5\right\} + \mathcal{O}(\varepsilon,\delta)\right] \qquad (2.31)$$

The complete formula in $O(\alpha_s)$ for $\sigma_{2jet}(\varepsilon,\delta)$ was derived in refs. (50), where it was shown that the $\mathcal{O}(\varepsilon,\delta)$ terms are numerically significant. Of course, $\sigma^{2jet}_{(\varepsilon,\delta)}$ is just a special example of a large number of calculable (i.e. finite) sub-cross-sections. Also the (ε,δ) prescription is not obligatory. For example, jets can be defined also by cuts on the minimum invariant mass of a pair of partons for example all y_{ij} satisfying $y_{ij} > y_Q^2$. Then one could also show that $\sigma_{n\text{-jet}}(y)$ so defined are calculable. The first of these cross-sections, $\sigma_{2jet}(y)$ was obtained in ref. (51), getting

$$\sigma^{2jet}(y) = \sigma^0\left[1 + 2\alpha_s(Q^2)/3\pi \times \left\{-2\ln^2 y - 3\ln y + 4y\ln y - 1 + \pi^2/3\right\} + O(y)\right] \qquad (2.32)$$

where again in any comparison with data, O(y) terms have to be included. Both eqs. (2.31) and (2.32) are $O(\alpha_s)$ proofs of the Kinoshita-Lee-Nauenberg theorem [52]. Since the proof of Sterman and Weinberg, the field of jet physics has made significant advances. Of special interest here are the calculations of $\sigma_{2jet}(y)$ in $O(\alpha_s)^2$ [53], and of $\sigma_{3jet}(y)$, $\sigma_{3jet}(\varepsilon,\delta)$ in $O(\alpha_s^2)$ [54] as well as $\sigma_{4jet}(y)$, $\sigma_{4jet}(\varepsilon,\delta)$ etc. [55] also in $O(\alpha_s)^2$. All these differential cross-sections are available in the form of numerical Monte Carlo programmes [56] and can be used

(and have been used) in the analysis of hadronic final states in e^+e^- annihilation.

A particularly compact expression for $\sigma_{2jet}(y)$ in $O(\alpha_s)^2$ has been obtained by Kramer and Lampe [53], which can also be used with appropriate modifications for the decays $Z^0 \to$ 2jets to extract $\alpha_s(Q^2)$. The result can be expressed as

$$\sigma_{2jet}(y) = \sigma^0 \Big[1 + 2\alpha_s(Q^2)/3\pi \times \{ -2\ln^2 y - 3\ln y + 4y\ln y - 1 + \pi/3 + O(y) \} + (\alpha_s(Q^2)/2\pi)^2 C_F \{ C_F Z_c + N_c Z_N + T_R Z_T + O(y) \} \Big] \qquad (2.33)$$

where

$$Z_c = 2\ln^4 y + 6\ln^3 y + (13/2 - 6\zeta_2)\ln^2 y + (9/4 - 3\zeta_2 - 12\zeta_3)\ln y + 1/8 - 51/4\,\zeta_2 + 11\zeta_3 + 4\zeta_4$$

$$Z_N = 11/3\ln^3 y + (2\zeta_2 - 169/36)\ln^2 y + (6\zeta_3 - 57/4)\ln y + 31/9 + 32/3\,\zeta_2 - 13\zeta_3 + 45/2\,\zeta_4$$

$$Z_T = -4/3\ln^3 y + 11/9\ln^2 y + 5\ln y + 19/9 - 38/9\,\zeta_2 \qquad (2.34)$$

and $C_F = 4/3$, $N_C = 3$, $T_R = n_{f/2}$ (n_f being the quarks) and ζ_n are the normal values of the zeta function, $\zeta_n = \sum_{k=1}^{\infty} k^{-n}$. The formula (2.33) has O(y) corrections, which are quite important numerically at least in $O(\alpha_s)$. Moreover, eq. (2.33) is not applicable for very small y values, where exponentiated form for (2.33) should be used. This is obtained by exponentiating the first two terms in $\sigma_{2jet}(y)$ in $O(\alpha_s)$ (which in $O(\alpha_s)^2$ then leads to the first two leading terms in Z_c in (2.34)). The exponentiated form is then applicable down to very small y values as shown in fig. (5). It can also be seen that the $O(\alpha_s^2)$ terms are

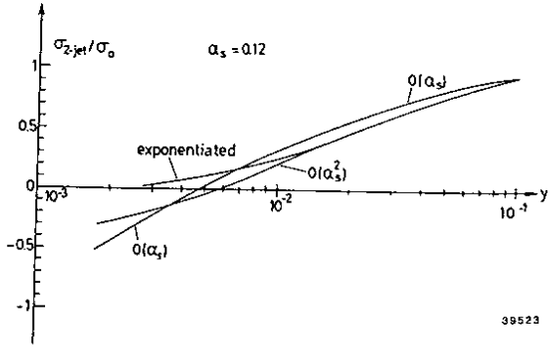

Fig. 5: Two-jet cross section $\sigma_{2\text{-jet}}(y)$ as a function of y in units of σ_0 for $\alpha_s = 0.12$. $O(\alpha_s)$ is exact lowest order result including all non-leading terms in y. $O(\alpha_s^2)$ is according to eq. (2.33) and "exponentiated" is the curve as described in the text.

small corrections on the leading order result. The formula (2.33) with the complete expression for $\sigma_{2jet}(y)$ in $O(\alpha_s)^2$ has been used in the analysis of $e^+e^- \to$ 2jet events from the JADE collaboration, yielding $\alpha_s(Q = 34\ \text{GeV}) = 0.12$, in agreement with expectations for $\Lambda_{\overline{MS}} = 0.1 - 0.2$ GeV. We shall not show here explicit formulae for $\sigma_{3jet}(y)$ or $_{3jet}(\varepsilon, \delta)$ which have been obtained analytically in $O(\alpha_s^2)$ upto O(y) or $O(\varepsilon, \delta)$ terms. It is now well appreciated that such 3-jet formulae have important numerical corrections, [54] which must be included in a reliable comparison of theory and experiment.

2.4 Energy Energy Correlations

We shall discuss in this section energy weighted two-particle correlations in the process $e^+e^- \to$ abx, introduced as a test of QCD by Basham, Brown, Ellis and Love [57], and popularly known as the Energy-Energy Correlations (EEC). The EEC can be visualized as the result of a measurement employing two calorimeters with the EEC defined as

$$1/\sigma \; d\Sigma/d\Omega\, d\Omega' \equiv 1/N \sum_{A=1}^{N} \left(1/Q \cdot d\Sigma^A/d\Omega\right)\left(1/Q \, d\Sigma^A/d\Omega'\right) \tag{2.35}$$

where $Q = \sqrt{s}$, the total energy, the label (= 1 to N) refers to the specific event, out of N events, and $d\Sigma^A/d\Omega$ and $d\Sigma^A/d\Omega'$ refer to the total energy measured in each event in each of the calorimeters. The normalization is such that

$$1/\sigma \int d\Sigma/d\Omega\, d\Omega' \; d\Omega\, d\Omega' = 1 \tag{2.36}$$

where self-correlations E_A^2 at 0° are also included. Of course, in an experiment E^A are constructed from the sum $E_A{}^a$ over the particles a whose momenta have relative angles χ (to $\chi+\Delta\chi$). In terms of perturbative QCD, the first non-trivial contribution to the EEC (i.e. for $\chi \neq 0^\circ, 180^\circ$) is due to the $O(\alpha_s)$ process $e^+e^- \to q\bar{q}g$. For the experimental configuration where the angle between the two calorimeters, χ, ($\Omega.\Omega' = \cos\chi$) and the polar angle of one of the calorimeters measured with respect to the e^+e^- axis, θ, are fixed, one has in $O(\alpha_s)$ [57]

$$1/\sigma_0 \; d^2\Sigma/d\cos\chi\, d\cos\theta = \alpha_s(Q^2)/\pi \left[a(\xi) + \cos^2\theta \; b(\xi) \right] \tag{2.37}$$

where

$$a(\xi) = 1/4(1-\xi)\left[\left(18/\xi^5 - 42/\xi^2 + 22/\xi^3\right)\ln(1-\xi) + 18/\xi^4 - 33/\xi^3 + 7/\xi^2 + 3/\xi + 2\right]$$

$$b(\xi) = 1/4(1-\xi)\left[\left(18/\xi^5 - 66/\xi^4 + 78/\xi^3 - 32/\xi^2\right) \times \ln(1-\xi) + 18/\xi^4 - 57/\xi^3 + 51/\xi^2 - 9/\xi - 6\right] \tag{2.38}$$

where $\xi = \frac{1-\cos\chi}{2}$ and it lies in the range $0 \leqslant \xi \leqslant 1$.

Experimentally, it is found much more convenient to integrate over the polar angle, θ, also, and obtain a single differential distribution in $\cos\chi$. The "average" EEC so obtained has a simple definition

$$1/\sigma \; d\Sigma/d\cos\chi = 2/(Q^2 \Delta\chi \sin\chi)\, 1/N \sum_{A=1}^{N} \sum_{\text{pairs}} E_A^a \, E_A^b \tag{2.39}$$

where a and b label individual particles. The result of integrating (2.37) over $\cos\theta$ can be simply expressed as

$$1/\sigma_0 \; d\Sigma/d\cos\chi = \alpha_s(Q^2)/\pi \; F(\xi) \tag{2.40}$$

where $F(\xi)$ is given by [57]

$$F(\xi) = (3-2\xi)/6\xi^5(1-\xi) \times \left[2(3-6\xi+2\xi^2)\ln(1-\xi) + 3\xi(2-3\xi)\right] \tag{2.41}$$

In fig. (6) we show the function $F(\xi)$. We remark that the function $F(\xi)$ is singular both for $\xi \to 1$ (i.e. $\chi \simeq \pi$) and $\xi \to 0$ ($\chi = 0$). The leading singularity is for the opposite side ($\chi = \pi$) correlation

$$F(\xi) \xrightarrow[\xi=1]{} 1/(1-\xi)\ln(1-\xi) \tag{2.42}$$

and this behaviour is singular by one power in $(1-\xi)$ as compared to the pure phase space case. Hence, perturbative QCD in fixed order in α_s cannot be arbitrarily pushed close to $\chi = 0$ and $\chi = \pi$ regions, something which is worth remembering by our experimental colleagues. A related quantity of interest is the asymmetric part of the "average" EEC defined as

$$d\Sigma^{Asym.}/d\cos\chi \equiv d\Sigma(180^\circ-\chi)/d\cos\chi - d\Sigma(\chi)/d\cos\chi \tag{2.43}$$

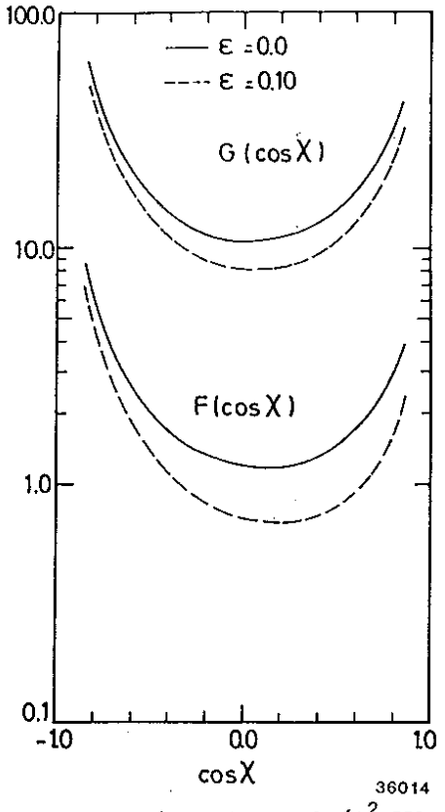

Fig. 6: The $O(\alpha_s)$ and $O(\alpha_s)^2$ EEC functions defined in the text. The solid curves correspond to the usual definitions of EEC with $\varepsilon = \delta = 0$, and the dashed curves correspond to an (ε,δ) cut-off $\varepsilon = 0.1$ and $\delta = (\min \theta_{ij}) = 26^0$.

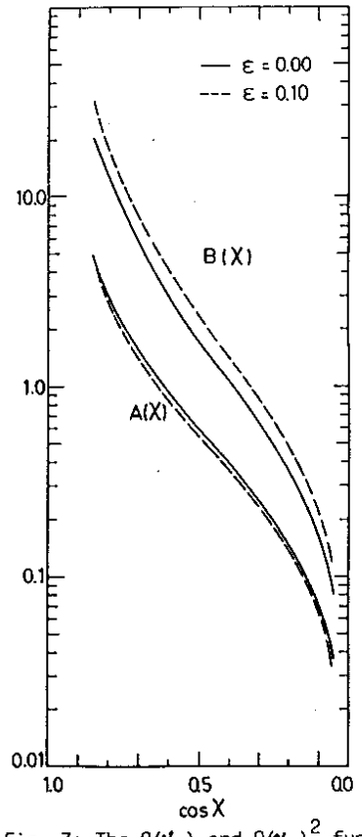

Fig. 7: The $O(\alpha_s)$ and $O(\alpha_s)^2$ functions for the asymmetry in EEC with the same notation as used in fig. 6.

In $O(\alpha_s)$,

$$1/\sigma_0 \, d\Sigma^{Asym.}/d\cos\chi = \frac{\alpha_s(Q^2)}{\pi} A(\bar{z}) \qquad (2.44)$$

where by definition

$$A(\bar{z}) \equiv F(1-\bar{z}) - F(\bar{z}) \qquad (2.45)$$

The function $A(\chi)$ is shown in fig. (7).

If one is away from the $\chi = 0$ and π angular regions, then one need not calculate the contributions from the processes $e^+e^- \to q\bar{q}$. To do a quantitative analysis of the data for $d\Sigma$ and $d\Sigma^{Asym.}$ (with $\chi \neq 0^0$, 180^0), one has to calculate the $O(\alpha_s)^2$ diagrams shown in fig. (8). Since we are primarily interested in the "average" EEC, the $O(\alpha_s)^2$ calculations amount to studying the processes $\gamma^* \to q\bar{q}g$, $q\bar{q}gg$ and $q\bar{q}q\bar{q}$ in that order. These corrections were obtained in refs. (58) and (59), from where we quote the results parametrized in the form

$$1/\sigma_0 \, d\Sigma/d\cos\chi = \alpha_s(Q^2)/\pi \, F(\bar{z}) + (\alpha_s(Q^2)/\pi)^2 G(\bar{z})$$

$$1/\sigma_0 \, d\Sigma^{Asym.}/d\cos\chi = \alpha_s(Q^2)/\pi \, A(\bar{z}) + (\alpha_s(Q^2)/\pi)^2 B(\bar{z}) \qquad (2.46)$$

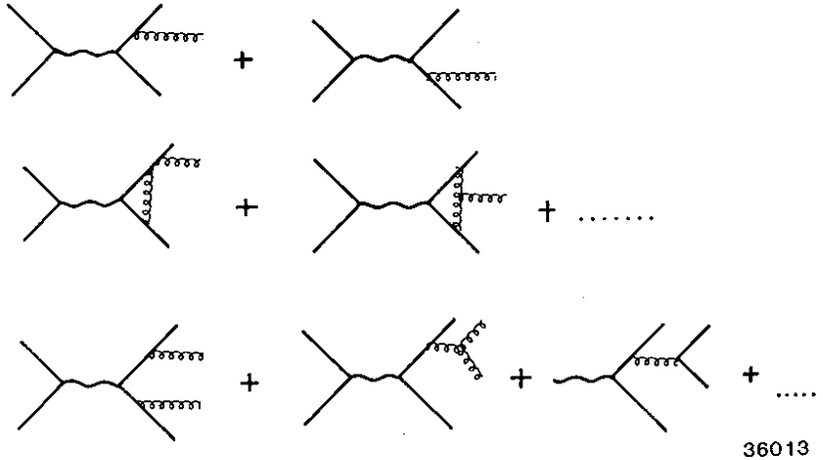

Fig. 8: Some diagrams contributing to the 3- and 4-jet processes upto $O(\alpha_s)^2$ in e^+e^- annihilation

The EEC and EECA functions $G(\cos\chi)$ and $B(\bar{z})\,(= G(1-\bar{z}) - G(\bar{z}))$ are also shown in figs. (6) and (7), respectively. To get an estimate

for the $O(\alpha_s)^2$ contribution, one can express the $O(\alpha_s)^2$ corrections in the form

$$1/\sigma \; d\Sigma/d\cos\chi = \alpha_s(Q^2)/\pi \left(1 + \alpha_s(Q^2)/\pi \, R^{Corr.}_{(3)}\right)$$

$$1/\sigma \; d\Sigma^{Asym.}/d\cos\chi = \alpha_s(Q^2)/\pi \times \left(1 + \alpha_s(Q^2)/\pi \, R^{Asym.}_{(3)}\right) \qquad (2.47)$$

Then, typically

$$R^{corr}(\zeta) = 8 - 10$$

$$R^{Asym}(\zeta) = 3 \qquad (2.48)$$

Thus, the $O(\alpha_s)^2$ corrections in $d\Sigma/d\cos\chi$ are substantial ($\sim$ 40 %) but they are small (O(10 %)) in $d\Sigma^{Asym}/d\cos\chi$. Since the quantity EEC does not require the identification of any jet, the changes in going over to $Z \to q\bar{q}g$, $q\bar{q}gg$, $q\bar{q}q\bar{q}$ are minimal, since the VA terms do not contribute. In figs. (6) and (7) we also show the effect of implementing a resolution on the parton energies and angles using the Sterman-Weinberg (ε, δ) parameters. Such estimates are needed for guessing infrared sensitivity. It is seen that the EEC functions $F(\zeta)$ and $G(\zeta)$ are both linearly dependent on the energy cut-off ε and hence are expected to receive large power corrections. The asymmetry functions $A(\zeta)$ and $B(\zeta)$ on the other hand are rather stable against (ε, δ) variations. The cumulative effect of ε variation on the asymmetry is shown in fig. (9) for ε in the range $0 < \varepsilon < 0.1$. The difference is hardly noticeable.

Thus, it seems that the asymmetry in the EEC, $d\Sigma^{A}/d(\cos\chi)$, is a reliable quantity for estimating $\alpha_s(Q^2)$ from e^+e^- data. Obviously, before such an exercise can be undertaken one has to estimate the genuine non-perturbative effects due to fragmentation. This, however, can only be modelled and not surprisingly there is no unanimity on that issue. One

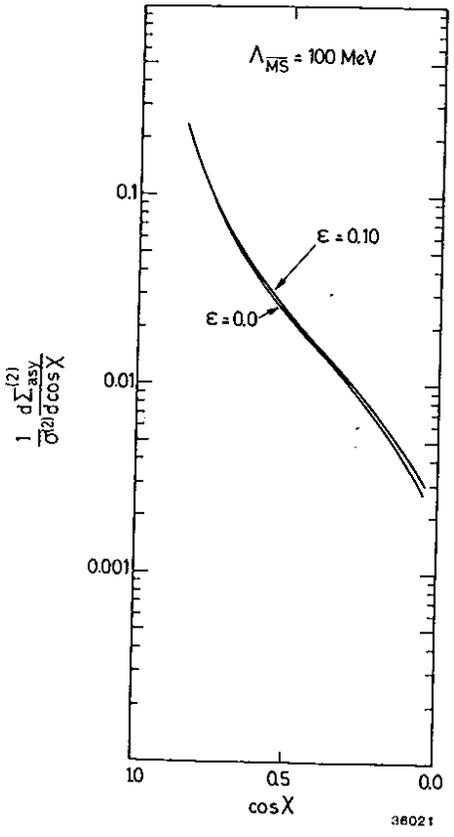

Fig. 9: The cross section in perturbative QCD calculated upto $O(\alpha_s)^2$ for $\Lambda_{\overline{MS}}$ = 100 MeV and $\sqrt{s}$ = 34 GeV for two values of the cut-offs (i) $\varepsilon = \delta = 0$, (ii) $\varepsilon = 0.1$, $\delta = 26^0$.

could use the data to guess the power corrections in a model independent way. For data from DESY experiments, this is shown in figs. (10), which suggest small power corrections in the integrated EECA. An estimate of the contribution of the fragmentation component in EECA for PETRA and LEP energies is shown in fig. 11, based on a so-called independent jet model. This suggests $\sim$ 10 % non-perturbative contribution to the integrated asymmetry with $\cos\chi < 0.8$ around $\sqrt{s} = m_Z$ = 92 GeV. The corresponding non-perturbative estimates in the present versions of the Lund fragmentation model are in comparison larger also at LEP energies, typically amounting to $\sim$ 20 %. Thus, it seems that the non-perturbative uncertainty in α_s determination in EECA would be reduced to a level of O (10 %) at LEP energies. The corresponding uncertainty is typically of O(25 %) at PETRA/PEP energies, resulting in $\alpha_s(Q^2)$ values which range between 0.12 and 0.16 for $Q^2 \simeq 1200$ GeV^2 (60).

Let us hope that there will be some progress in the understanding of non-perturbative effects in the meantime. In any case, fragmentation effects, being power corrections of sorts, have to become weaker with increasing $\sqrt{s}$. By the same token, the sensitivity of data on the QCD parameter Λ will also decrease at LEP energies.

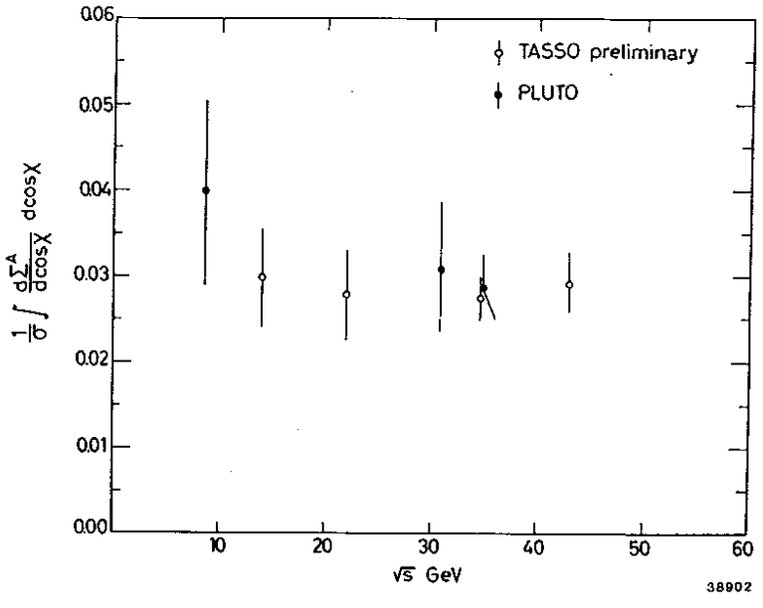

Fig. 10 (a): The integrated EEC data (points) of the TASSO and PLUTO collaboration (from ref. (1))

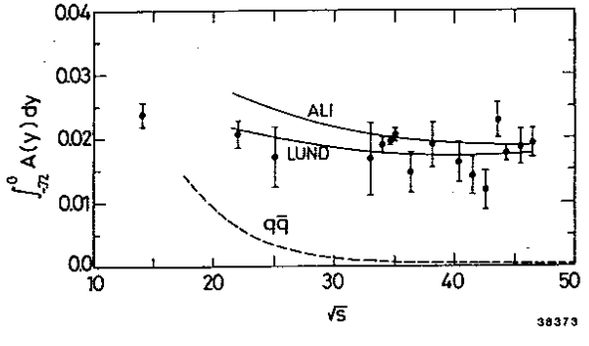

Fig. 10 (b): The integrated EECA data (points) of MARK J together with the $q\bar{q}$ contribution (dashed curve) are shown as function of $\sqrt{s}$. The Monte Carlo predictions of two models for $\Lambda_{\overline{MS}}$ = 100 MeV are shown as solid curves (from ref. 60)

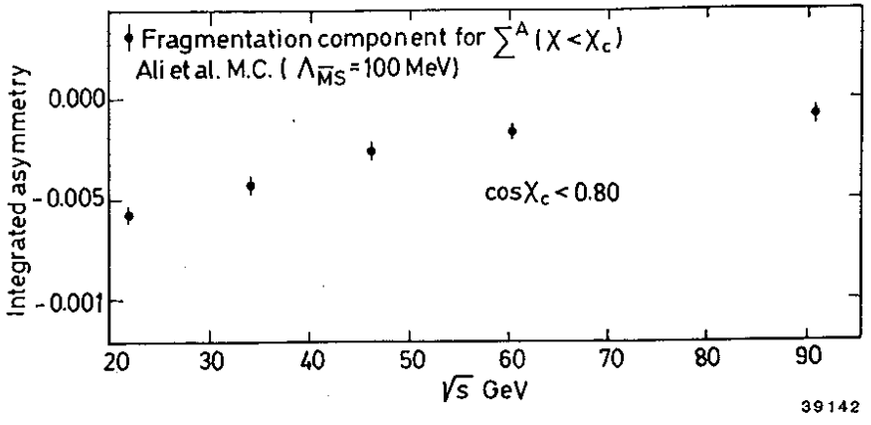

Fig. 11: Energy (s) dependence of the fragmentation component of the integrated asymmetry in EEC with the indicated parameters, in the model of ref. (56)

The EEC function has also been evaluated for large χ values, χ close to π, in the leading log approximation [61]. The analytic form agrees also with the numerical Monte Carlo programme of Weber [62], which takes into account coherence effects due to multiple gluon emission [63].

Including multiple gluon emissions, which essentially provide Sudakov type suppressions, extends the range of applicability of perturbative QCD and provides a better framework in approaching the non-perturbative regions. Of course, for parton virtuality approaching typical hadronic scales, O(1-2 GeV), non-perturbative effects must be included. A unified description of final states incorporating the sophisticated $O(\alpha_s)^2$ perturbation theory machinary applicable for large parton virtuality and coherence effects, predicted by QCD for small virtualities, is still missing.

We shall refrain from a detailed discussion of the stability of other jet measures and shape variables against $O(\alpha_s)^2$ and non-perturbative contributions. There is now a general consensus that $O(\alpha_s)^2$ corrections depend on the variable, hence a general statement about the stability

of jet (or gluon radiation) measures cannot be made. Examples of perturbatively stable quantities in e^+e^- annihilation are $\sigma_{tot}, \sigma_{2jet}(y)$, EECA, and oblateness, examples of quantities receiving substantial corrections in next to leading orders are variables like EEC, thrust and the Fox-Wolfram shape variables [64]. Having enough orders in $\alpha_s(Q^2)$, perhaps all these variables would have the same significance at the perturbation theory level. These, however, have still to be calculated beyond $O(\alpha_s)^2$. Pending such higher order calculations, it is only sensible to use such variables for the determination of $\alpha_s(Q^2)$ where the stability of the perturbation series has been demonstrated.

2.5 Test of the Nonabelian Character of QCD

In this section we briefly recapitulate the tests for the nonabelian couplings in QCD suggested in the processes $e^+e^- \to \gamma, Z \to 4$ jets and in orthotoponium decays, $\theta \to 4$ jets, $\gamma + 3$ jets. In particular, the large event rates at the Z^0 should enable us to obtain a significant sample of 4-jet events. Moreover, due to the high energy (~ 92 GeV), the separation of 4-jet events from the more frequent 2- and 3-jet events should be lot easier than at presently available energies (29-45 GeV) at PETRA and PEP.

The 3-gluon vertex in QCD can be tested by comparing QCD with an abelian version of "QCD", in which the vector gluons carry no colour, in analogy to the photon. Quarks still appear in 3 colours in order to agree with the measured value of R. Both QCD and "QED" yield the same 3-jet rate if the couplings are related by $\alpha_{"QED"} = \frac{4}{3}\alpha_{QCD}$. In "QED", [65] the diagram with the triple gluon coupling in fig. (8) is switched off and to be consistent, the 4-quark cross-section in $e^+e^- \to q\bar{q}q\bar{q}$ has to be multiplied by 8. This is the essential difference in the 4 jets, namely the relative contributions of the states $e^+e^- \to q\bar{q}gg$ and $e^+e^- \to q\bar{q}q\bar{q}$ in "QED" and QCD are different. Roughly speaking, in inclusive 4jet cross-sections the ratio $\frac{\sigma(e^+e^- \quad q\bar{q}gg)}{\sigma(e^+e^- \quad q\bar{q}q\bar{q})}$ is about 10 and 1 in QCD and QED, respectively. Since the process $e^+e^- \to q\bar{q}gg$ is more singular (both in QCD and "QED") than $e^+e^- \to q\bar{q}q\bar{q}$, one expects this aspect to be emphasized lot more in QCD than in "QED" type theories.

In the decays of orthotoponium, the decays $\theta \to gggg$ are allowed only in QCD. However, the decays $\theta \to gg q\bar{q}$ are allowed in both QCD and "QED". Again, the difference, apart from the overall rate, lies in the intrinsic distributions in $\theta \to gggg$ decays as against the ones in $\theta \to gg q\bar{q}$. The same qualitative statements apply to the decays $\theta \to \gamma +$ 3 jets, which in "QED" type theories arise from $\theta \to \gamma + g + q\bar{q}$.

We shall first discuss the case $e^+e^- \to \gamma, Z \to 4$ jets. Defining jets by the Sterman-Weinberg variables ε, δ, one expects that for $\alpha_s(92\text{ GeV}) = 0.1$, $\sigma_{4jet}(\varepsilon = 0.15, \delta = 35^0) \sim 4$ %. Even with the rather stringent cut-offs indicated here, one expects $\sim 4 \times 10^4$ $Z^0 \to$ 4jet events per 10^6 hadronic decays of the Z^0. Thus, 4 jet rates are not going to be any problem at the Z^0. There are two distributions that have been studied. The first is the distribution in the azimuthal angle, ϕ, defined by Körner, Schierholz and Willrodt [66],

$$\cos\phi = \vec{n}_1 \cdot \vec{n}_2 \tag{2.49}$$

where the normals n_1 and n_2 are defined for the configurations with each hemisphere consisting of two jets

$$\vec{n}_1 \equiv (\vec{P}_1 \times \vec{P}_2)/(|\vec{P}_1||\vec{P}_2|)$$
$$\vec{n}_2 \equiv (\vec{P}_3 \times \vec{P}_4)/(|\vec{P}_3||\vec{P}_4|) \tag{2.50}$$

The normalized distributions in ϕ for the oriented (i.e. energy ordered) 2-2 configuration for QCD and "QED" type theories are shown in fig. (12), where results for more relaxed cuts ($\varepsilon = 0.1, \delta = 25^0$) are also presented. The QCD curves shows the characteristic enhancement near 180^0, where the two lower energetic partons, preferentially the gluons, are close together. The "QED" distribution is rather flat. The statistical significance of the test may be expressed through the average value $\langle\phi\rangle$

	$\varepsilon = 0.1, \delta = 25^0$	$\varepsilon = 0.15, \delta = 35^0$
QCD	97.0 ± 0.5^0	97.7 ± 0.9^0
"QED"	91.5 ± 0.6^0	90.3 ± 0.9^0

With 10^5 hadronic events, the distinction between the two theories amounts

to 8σ even with the stringent cut offs.

The other distribution, due to Nachtmann and Reiter [67], aims at studying the different helicity structure of the $G^* \to GG$ and $G^* \to Q\bar{Q}$ vertices in fig. (8). The distribution in the variable θ_{31} defined as the angle between the axis of two almost antiparallel partons of high energy (1 and 2) and of the axis of the other two almost antiparallel partons of lower energies (3 and 4), with the ordering $E_1 > E_2 > E_3 > E_4$ is sensitive to the splitting $G^* \to GG$ and $G^* \to Q\bar{Q}$. For reasons of experimental ease, we have however introduced a modified angle, $\bar{\theta}_{31}$, which is defined as follows

$$\cos\bar{\theta}_{13} = \vec{n}_{12} \cdot \vec{n}_{34} \qquad (2.51)$$

with

$$n_{12} \equiv \left(\vec{P}_1/|\vec{P}_1| - \vec{P}_2/|\vec{P}_2|\right)$$

$$n_{34} \equiv \left(\vec{P}_3/|\vec{P}_3| - \vec{P}_4/|\vec{P}_4|\right)$$

There were two additional cuts introduced on the 4-jet event sample, namely we require $E_3/E_2 < 1/2$ and $\cos\theta_{34} < -0.7$. These cuts reduce the 4-jet sample enormously, leaving only about 6 % of all 4 jet events generated with the indicated (ε, δ) values. The normalized distributions $d\sigma/d|\cos\bar{\theta}_{13}|$ for QCD and "QED" type theories are shown in fig. (13) for the (ε, δ) values indicated. The two distributions are distinguishable. Again, the significance of the test can be indicated through the average value $\langle|\cos\bar{\theta}_{13}|\rangle$

	$\varepsilon = 0.1,\ \delta = 25^0$	$\varepsilon = 0.15,\ \delta = 35^0$
QCD	0.627 ± 0.007	0.483 ± 0.014
QED	0.545 ± 0.008	0.445 ± 0.012

The statistical significance of this test is comparable to that of the KSW method. For estimates of background from the fragmentation process, as well as from the decay $Z^0 \to t\bar{t} \to$ jets we refer to the detailed report by Rudolph [13].

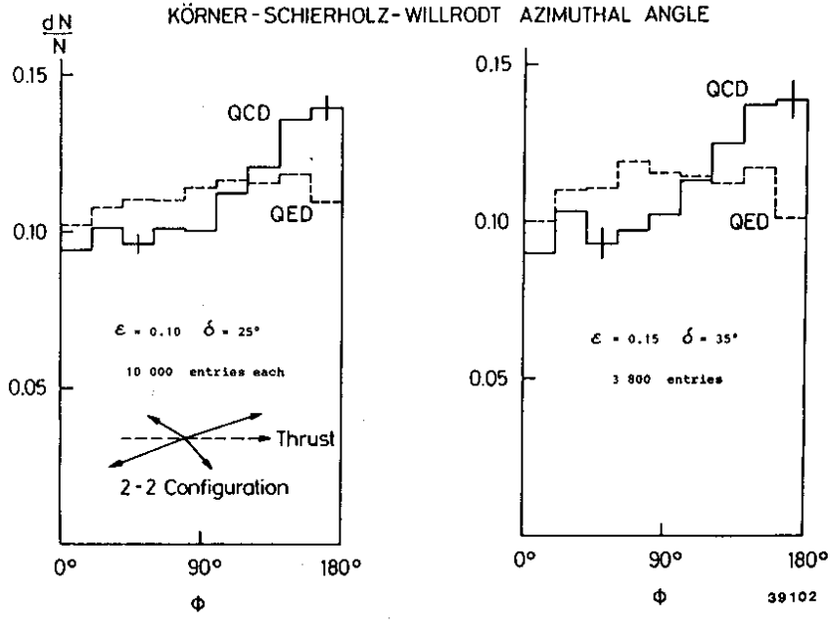

Fig. 12: Normalized distributions in the Körner-Schierholz-Willrodt azimuthal angle, ϕ, for the QCD and "QED" type theories.

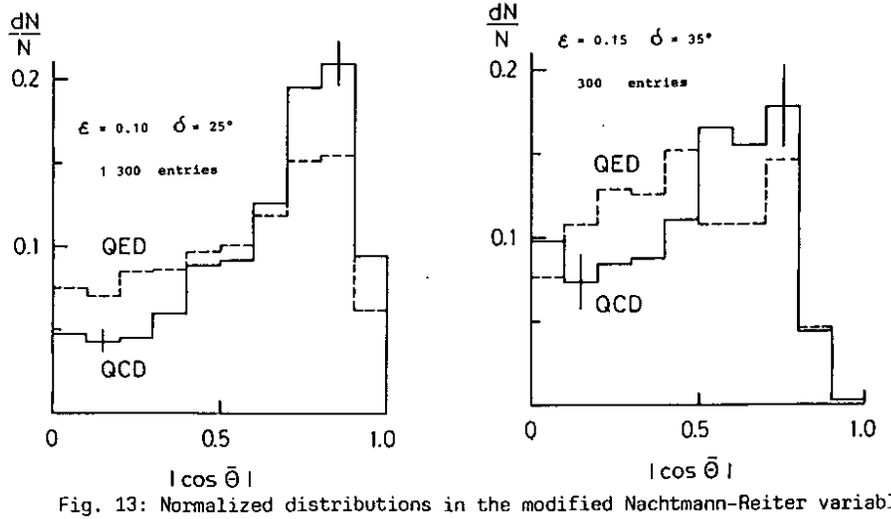

Fig. 13: Normalized distributions in the modified Nachtmann-Reiter variable $|\cos\bar{\theta}_{31}|$ for QCD and "QED" type theories

Next, we discuss the tests of the non-abelian nature in orthotoponium decays $\theta \to$ 4jets, and $\theta \to \gamma$ + 3jets. Since, as the top quark mass increases the single quark decays of the top quark in θ (= $t\bar{t}$) become dominant, the branching ratios for the QCD processes $\theta \to$ 3jets, 4jets etc. decrease. In addition, since the ratio R for 60 GeV $\gtrsim \sqrt{s} \gtrsim$ 80 GeV (expected value of m_θ) is rather large, there would be copious production of 3 and 4jet events from the non-resonating background $e^+e^- \to \gamma$, $Z \to$ 3jets, 4jets. The rather large value of m_θ has introduced some non-trivial complications in carrying out the simple QCD tests suggested for the $\theta \to$ 3jets, 4jets final state. This problem deserves further theoretical study. If, however, it turns out that $m_\theta \simeq m_Z$, then since $\Gamma(Z) \gg \Gamma(\theta)$, the processes $e^+e^- \to \gamma$, Z, $\to$ 3 jets, 4jets will be dominated by the decays $Z^0 \to$ 3jets, 4jets and the tests that we have just described also hold for this situation. Because of this reason we have concentrated on the radiative decays $\theta \to \gamma$ + 3jets. In discussing these radiative decays, it is instructive to look at the Altarelli-Parisi splitting formula

$$D_{G \to GG}(z,\chi) = 6/2\pi \left\{ (1-z+z^2)^2/(z(1-z)) + z(1-z)\cos 2\chi \right\}$$

$$D_{G \to q\bar{q}}(z,\chi) = n_f/2\pi \left\{ 1/2\left[z^2+(1-z)^2 \right] - z(1-z)\cos 2\chi \right\} \qquad (2.52)$$

with n_f being the number of quark flavours, z is the momentum fraction of the outgoing parton and χ is the angle of (GG) or ($q\bar{q}$) plane with the linear polarization of the splitting gluon. One expects the dominance of the γGGG final state over $\gamma Gq\bar{q}$, since $D(G \to GG)$ is more singular than $D(G \to q\bar{q})$ near $z \simeq 0$. Since the virtual gluon in $\theta \to \gamma GG^* \to GG$ or $q\bar{q}$ is partly polarized perpendicular to the γGG^* plane, one also expects from the sign of this term in (2.52) that the GG plane tends

to be perpendicular to the γG plane whereas $q\bar{q}$ lies in the same plane. The most suitable angle to study this asymmetry in γ + 3jet events is the angle χ, between the normal to the plane given by the photon and the fastest jet in the hadronic rest frame and the normal to the plane of the other two jets. It turns out that there are clear differences between QCD and the "QED" (= $\gamma Gq\bar{q}$) events as shown in fig. 14 despite influence of the invariant mass cuts to define the jets.

An interesting distribution involves the polar angle, between the beam axis and the photon. This is shown in fig. (15), where we have shown the dependence of the quantity α defined as $d\Gamma/d\cos\theta \sim 1 + \alpha\cos^2\theta$ as a function of m_{min} (minimum invariant mass/m_θ per event). In an abelian (= $\gamma Gq\bar{q}$) theory one expects a strong decrease of α at large m_{min} contrary to QCD. The problem in this test is probably the rate since the branching ratio for $\theta \to \gamma$ + 3jets is not expected to be larger than 1 % for $m_\theta \gtrsim$ 80 GeV. A detailed calculation for the rates assuming various m_{min} cut-offs can be seen in the report by Streng [14].

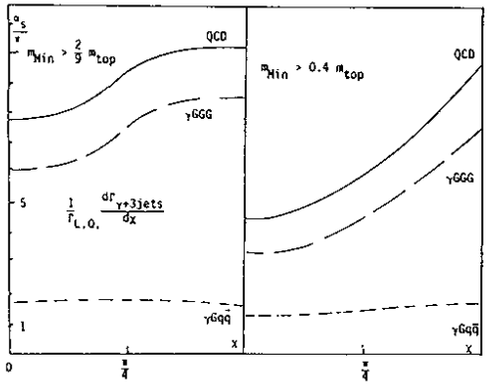

Fig. 14: The azimuthal angle distribution $\frac{1}{\Gamma_{L.O.}} d\Gamma_{\gamma+3jets}/d\chi$ for two m_{min} values

a) $m_{min} \gtrsim 2/9\ m_{top}$

b) $m_{min} \gtrsim 0.4\ m_{top}$

$\Gamma_{L.O.}$ is the decay width for $\theta \to \gamma GG$ with the same m_{min} cut-offs.

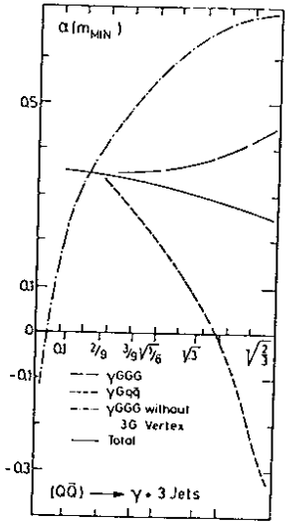

39110

Fig. 15: Average value of the photon polar angle coefficient α for jets as a function of m_{min}.

3. $\gamma\gamma$ Physics at LEP

We shall be brief in this section, since the reports on the measurements of the photon structure function, $F_2^{\gamma}(Q^2)$, by Cordier [16] and on the inclusive hadron production in $\gamma\gamma \to hX$ by Aurenche et al. [17] are sufficiently detailed and contain all essential formulae needed in comparison of theory with experiments at LEP energies. In addition, there exist some exhaustive review articles on two-photon physics [68),(69)], which contain systematic surveys of both the classical and recent developments in experimental and theoretical studies of this subject. For earlier studies of $\gamma\gamma$ physics at LEP see refs. (70). We shall restrict ourselves to elucidating some of the comments made in the introduction; some results from (16) and (17) are also presented and discussed.

3.1 Differential Photon Luminosities

We start with a discussion of the prototype 2γ process $e^+e^- \to e^+e^-x^0$. The differential cross-section for which can be written as [68]

$$d\sigma(e^+e^- \to e^+e^-X)/dQ_1^2 dQ_2^2 dx_1 dx_2 = d\mathcal{L}/dQ_1^2 dQ_2^2 dx_1 dx_2 \, \sigma_{\gamma\gamma}(W^2) \qquad (3.1)$$

where $\sigma_{\gamma\gamma}$ is the $\gamma\gamma \to x^0$ cross section of producing a final state with the mass, W. The variables are defined as follows

$$\left.\begin{aligned} x_i &= (E_{beam} - E_i'))/E_{beam} \\ Q_i^2 &= q_i^2/s \end{aligned}\right] \quad i = 1,2$$
$$z = W/\sqrt{s} \qquad (3.2)$$
$$K = z^2 + Q_1^2 + Q_2^2$$
$$\mathfrak{z}^2 = K^2 - 4Q_1^2Q_2^2$$

The differential transverse luminosity function is given by

$$d\mathcal{L}/dQ_1^2 dQ_2^2 dx_1 dx_2 = \alpha^2/16\pi^2 \; \mathfrak{z}/Q_1^2Q_2^2 \left\{ \left[\frac{K - 2(x_2 + Q_2^2)}{\mathfrak{z}^2} \right]^2 + 1 - \frac{m_e^2}{E^2Q_1^2} \right\} \times \left\{ \left[\frac{K - 2(x_1 + Q_2^2)}{\mathfrak{z}^2} \right]^2 + 1 - \frac{m_e^2}{E^2Q_2^2} \right\} \qquad (3.3)$$

Exact analytic expressions for the single differential distribution are available in the literature [71]. The luminosity function $d\mathcal{L}/dz$ is shown in fig. (16) for E_{beam} = 1000, 100, 15 GeV (curves A,B,C, respectively). The curves D and E correspond, respectively, to the differential luminosity in the so called single tag and double tag experiments for (with $0 < \phi < 2\pi$, $20 < \theta < 200$ mrad.) E_{beam} = 15 GeV (typical PETRA/PEP) energies. The steep rise near small values of z, and the slow beam energy dependence are the main features. Note the decrease in counting rates as one goes from no tag (curve C) to single tag (curve D) and double tag (curve D) experiments, which though shown for PETRA/PEP energies is also indicative of LEP-2γ experiments.

In having handy estimates for cross-sections and differential distributions it is customary to use the so called equivalent photon approximation, EPA [72]. This approximation ignores the fact that the photons are not quite on shell and not completely transverse. The limitation for the validity of EPA is Q_1^2, $Q_2^2 \ll z^2$. The Q_i^2 integration can then be performed analytically leading to the following expression for the differential luminosity

$$d^2\mathcal{L}/dx_1 dx_2 = n_\gamma(x_1, \theta_1^{max.}) \, n_\gamma(x_2, \theta_2^{max.}) \qquad (3.4)$$

The luminosity function factorizes into the product of two photon flux factors each depending on the angles and energies of only one of the two scattered electrons. Taking the limit $\theta^{max} = \pi$, $x \ll 1$

$$n_\gamma^{tot}(x) = 2\left(\frac{\alpha}{\pi}\right)^2 \frac{1}{x}\left(\ln(2E/m_e x) - 1/2\right)$$

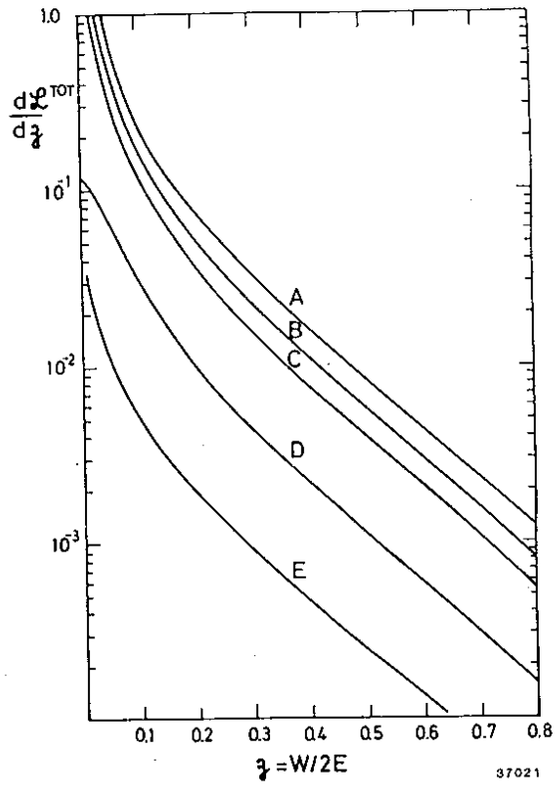

Fig. 16: Differential two photon luminosity functions. Curves A,B,C: total luminosity for E = 1000, 100, 15 GeV. Curve D: single tag luminosity function for $0 \leq \phi \leq 2\pi$, $20 < \theta < 200$ mrad. E = 15 GeV. Curve E: Double tag luminosity function for $0 \leq \phi \leq 2\pi$, $20 < \theta < 200$ mrad. E = 15 GeV

The condition Q_1^2, $Q_2^2 \ll z^2$ implies that either $\theta \ll 1$ or $x \simeq 1$. In either case the scaled mass of the photon photon system simplifies to $z^2 = W^2/s = x_1 x_2$. In the EPA approximation, the cross-section for the process $e^+e^- \rightarrow e^+e^- x^0$ can now be simply expressed as

$$d\sigma = d\mathcal{L}(E,W)/dW \; \sigma_{\gamma\gamma}(W)\, dW \qquad (3.5)$$

where the luminosity functions $d\mathcal{L}/dW$ for various tagging configurations are given in ref. 68.

The concept of $\gamma\gamma$ luminosity function is very useful; having it at hand, estimates of event rates in a given process $\gamma\gamma \rightarrow X(W)$ are trivial given $\sigma_{\gamma\gamma}(W)$. In particular, the relative efficiency of a machine, like for example that of PEP/PETRA in $\gamma\gamma$ physics can be compared with that of LEP or any other machine. As an example, it is instructive to compare the 'potential for new physics' in the $gg \rightarrow X$ subprocess in $\bar{p}p$ (pp) colliders with that in the $\gamma\gamma \rightarrow X$ process in e^+e^- colliders (fig. 17). Since one expects

$$\sigma_{\gamma\gamma}(W) \propto \left(\frac{\alpha^2}{W^2}\right), \quad \sigma_{gg}(W) \propto \left(\frac{\alpha_s^2}{W^2}\right) \qquad (3.6)$$

it seems fair to compare the quantities

$$\frac{\alpha^2}{W^2}\, d\mathcal{L}^{\gamma\gamma}/dW \quad \text{and} \quad \alpha_s^2/W^2\, d\mathcal{L}^{gg}/dW \qquad (3.7)$$

which have the canonical dimensions of a cross-section. The result of the calculation of $d\mathcal{L}^{gg}/dW$ based on the structure function of ref. (73) and $d\mathcal{L}^{\gamma\gamma}/dW$ in the EPA are shown in fig. (18). It is fair to conclude that the potential of the existing CERN $\bar{p}p$ collider with $\sqrt{s} \gtrsim 540$ GeV in the search of new particles exceeds that of LEP in $\gamma\gamma$ collisions by several orders of magnitude. However, such comparisons don't quite tell the entire story! A counter example where $\gamma\gamma$ collisions at LEP are superior compared to $\bar{p}p$ colliders is in the search of photinos and selectrons[74]. The supersymmetric analogue of the QED Compton process $\gamma e \rightarrow \gamma e$, namely $\gamma e \rightarrow \tilde{\gamma} \tilde{e}$, has been used at PEP and PETRA to search for e practically upto $m_{\tilde{e}} \lesssim 1.8\, E_{beam}$ [75]. Experiments at LEP with good γ-tagging can explore a very large region in $m_{\tilde{e}} - m_{\tilde{\gamma}}$ plane as compared to the CERN collider, which is better suited for the search of scalar quarks and gluinos [76]. We shall not enter into the details of $\tilde{e}$ and $\tilde{\gamma}$ searches at LEP, since this topic is being covered by the working group on new particles at LEP [77].

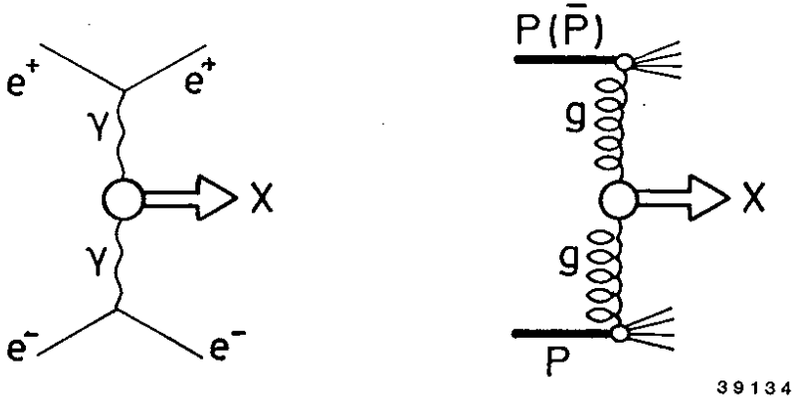

Fig. 17: versus gluon gluon collisions

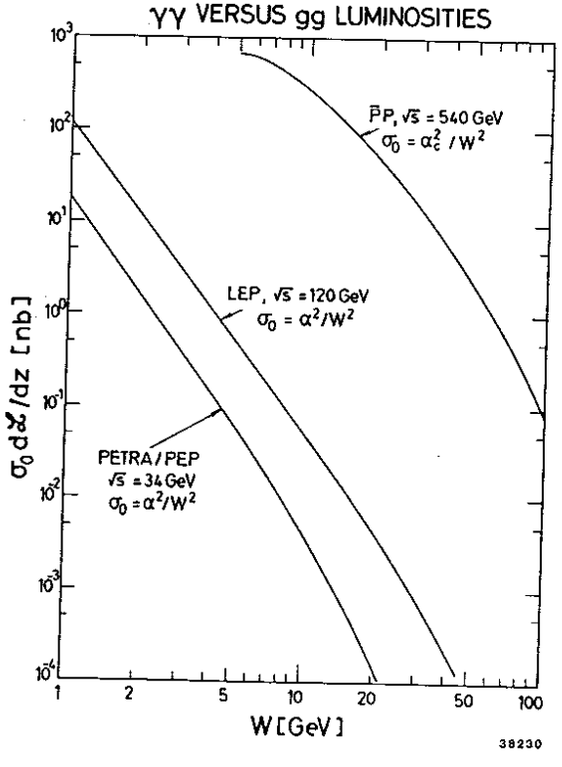

Fig. 18: Comparison of $\gamma\gamma$ and gluon gluon luminosities in e^+e^- and $\bar{p}p$ colliders (from ref. 23)

3.2 Single Resonance Production

The simplest two photon process is that in which two virtual photons annihilate to give a state R of definite spin and parity

$$e^+e^- \to Re^+e^- \tag{3.8}$$

The spin-parity selection rules as well as the helicity structure of the cross-sections are discussed in detail in ref. (68). The cross-section for $\gamma\gamma \to R$ can be expressed in terms of the radiative width $\Gamma(R\to\gamma\gamma)$ and the total width of the resonance R, Γ_W, by

$$\sigma^{(W)}_{\gamma\gamma\to R} = \frac{8\pi(J_R+1)(m_R/W)^2\,\Gamma_{\gamma\gamma}(R)\,\Gamma_W}{(W^2-m_R^2)^2 + m_R^2\,\Gamma^2(W)} \tag{3.9}$$

where J_R is the spin of the resonance R. In the EPA, one can show that the cross-section $\sigma^{tot}(e^+e^-\to e^+e^-R)$ is given by

$$\sigma(e^+e^-\to e^+e^-R) = 16\alpha^2/m_R^3 \ln(2E/m_e)^2 \times f(m_R/2E)(2J_R+1)\,\Gamma_{\gamma\gamma}(R) \tag{3.10}$$

where f(x) is the luminosity function and is also given by [78]

$$f(x) = (2+x^2)^2 \ln(1/x) - (1-x^2)(3+x^2) \tag{3.11}$$

[for R = 0^-, one has instead $(2+x)^2 \ln 1/x$ due to a kinematic factor originating in the 0^- matrix element, for practical interest $x \ll 1$, it hardly matters]. The expression (3.10) is approximate in the sense that it neglects the Q^2 dependence of form factors as well as interference effects of various resonances. In any case eq. (3.10) is the basis for a large number of measurements of $\Gamma_{\gamma\gamma}(R)$ in $\gamma\gamma$ collisions in existing e^+e^- machines. The present status of this subject is reviewed in ref. (11). For the sake of completeness we give here the radiative widths for the Higgs boson and pseudoscalar hypermeson. The effective $H^0 \to 2\gamma$ coupling can be expressed as (: k_1, k_2, ϵ_μ and ϵ_ν are the momenta and polarization vectors of the two photons)

$$F(K_1, K_2) = 2\alpha/(\pi\langle\phi\rangle) I_{\mu\nu}(k_1, k_2) \times \epsilon_\mu \epsilon_\nu \quad (3.12)$$

where $\langle\phi\rangle \simeq$ 250 GeV. Gauge invariance dictates that $I_{\mu\nu}$ be expressed as

$$I_{\mu\nu} = (k_{1\mu} k_{2\nu} - k_1 \cdot k_2 g_{\mu\nu}) I \quad (3.13)$$

then [79]

$$\Gamma(H^0 \to 2\gamma) = G_F \alpha^2/(8\pi\sqrt{2}) m_H^3 |I|^2 \quad (3.14)$$

For three generations, one has $I \simeq 0.7$. This gives a width of $\sim 10^{-2}$ eV for $m_{H^0} \simeq 1$ GeV rising to ~ 8 eV for $m_{H^0} \sim 10$ GeV. (For comparison $\Gamma(\pi^0 \to 2\gamma) \simeq 7.4$ eV). The relative cross-section for $\sigma(e^+e^- \to e^+e^- H^0)$ can then be obtained from $(e^+e^- \to e^+e^- \pi^0)$ from the expression

$$\frac{\sigma(e^+e^- \to e^+e^- H^0)}{\sigma(e^+e^- \to e^+e^- \pi^0)} = \frac{f(m_H/\sqrt{s})\, \Gamma_{\gamma\gamma}(H^0)}{f(m_{\pi^0}/\sqrt{s})\, \Gamma_{\gamma\gamma}(\pi^0)} \quad (3.15)$$

which gives a factor $\sim 10^{-3}$ for $m_{H^0} \sim m_{\pi^0}$. Despite the m_H^3 dependence of $\Gamma_{\gamma\gamma}(H^0)$ on m_{H^0}, the suppression due to the luminosity factor is more than offsetting. Thus, the prospects of Higgs searches in $\gamma\gamma$ collisions are not very bright.

The case of hyperpion, π'^0 production in $\gamma\gamma$ collisions, apart from the obvious difference in mass and couplings, can be treated exactly like that of $\gamma\gamma \to \pi^0$. The decay width $\pi'^0 \to 2\gamma$ can be expressed as [80]

$$\Gamma(\pi'^0 \to \gamma\gamma) = \frac{f^2_{\gamma\gamma\pi'}}{64\pi} m^3_{\pi'^0} \quad (3.16)$$

where the $f_{\gamma\gamma\pi'}$ coupling is defined via the amplitude

$$m(\pi'^0 \to 2\gamma) = f_{\gamma\gamma\pi'} \epsilon_{\mu\nu\lambda\sigma} k_1^\mu k_2^\nu \epsilon_1^\sigma \epsilon_2^\rho \quad (3.17)$$

The width $\Gamma(\pi'^0 \to 2\gamma)$ can be expressed in terms of $\Gamma(H^0 \to 2\gamma)$ (for $m_H = m_{\pi'^0}$)

$$\Gamma(\pi'^0 \to 2\gamma)/\Gamma(H^0 \to 2\gamma) = N_c'^2 n_f'/(36\pi^2 |I|^2) \quad (3.18)$$

which for N_c' (= number of hypercolour) = 3 and n_F' (= number of hyperflavours) = 6 is of O(1). Thus, the production of a hyperpion, π'^0, in $\gamma\gamma$ collisions seems equally unlikely.

Returning to the production of ordinary hadrons in $\gamma\gamma$ collisions, another area of considerable theoretical interest is in the production of exclusive states, like for example $\gamma\gamma \to \pi^+\pi^-$, K^+K^-, $K^0\bar{K}^0$, $p\bar{p}$, ... The exclusive two body processes $\gamma\gamma \to H\bar{H}$ at large $W^2_{\gamma\gamma}$ and fixed $\theta_{c.m.}$ provide a particularly interesting area for the application of perturbative QCD. The large momentum transfer behaviour, helicity structure, and in some cases even the overall normalization can be predicted from QCD [81]. The $\gamma_\lambda \gamma_{\lambda'} \to H\bar{H}$ amplitude can be written in a factorized form

$$m_{\lambda\lambda'}(W, \theta_{c.m.}) = \int_0^1 |dy_i|\, \phi_H(x_i, \hat{Q}) \phi_{\bar{H}}(y_i, Q^2)\, T_{\lambda\lambda'}(x, y; W, \theta_{c.m.}) \quad (3.19)$$

where $T_{\lambda\lambda'}$ is the hard scattering helicity amplitude for scattering the clusters of valence quarks in each hadron and ϕ_H are the probability amplitudes for finding valence quarks in the hadron each carrying the fraction x_i of the hadron's momentum. They require input from non-perturbative bound state physics, but their Q^2 dependence is calculable in QCD. In some cases the normalization and angular behaviour are insensitive to the precise form of these wave functions. For example one can show [81],

$$\frac{d\sigma/dt(\gamma\gamma \to \pi^+\pi^-)}{d\sigma/dt(\gamma\gamma \to \mu^+\mu^-)} \simeq \frac{4|F_\pi(Q^2)|^2}{1 - \cos^4\theta_{c.m.}} \quad (3.20)$$

where $F_\pi(Q^2)$ is the pion form factor. Recent data from PEP and PETRA have led to precise tests of the form (3.20) for hadron pair mass upto 3 GeV. This is a flourishing area of $\gamma\gamma$ physics and certainly is also suitable for studies at LEP. We shall, however, not go in the details and refer to recent reviews in literature.

3.3 Deep Inelastic Photon Scattering

The next class of processes in $e^+e^- \rightarrow e^+eX^0$ are the ones which involve $x = q\bar{q}$. There are two basic kinematic domains of interest here as shown in fig. (19). The two photon process $e^+e^- \rightarrow e^+e^-\gamma\gamma \rightarrow e^+e^-q\bar{q}$ shown in fig. 19(a) is characterized by small q_1^2, t_1^2 and large q_2^2 values. This

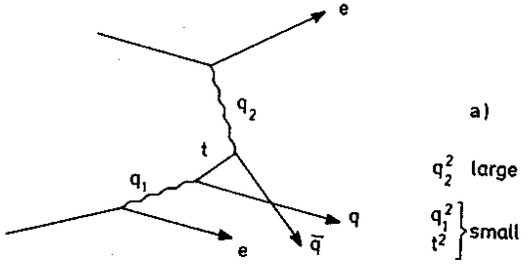

a)

q_2^2 large

q_1^2, t^2 } small

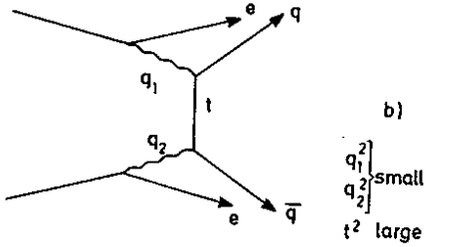

b)

q_1^2, q_2^2 } small

t^2 large

Fig. 19: Kinematic configurations for
a) Deep inelastic γ scattering
b) Large-p_T production of hadrons in $\gamma\gamma \rightarrow q + \bar{q}$

then provides the kinematic configuration to study the deep inelastic scattering of a highly virtual photon ($m_\gamma^2 = q_2^2$, large) on an almost

on-shell photon target ($m_\gamma^2 = q_1^2 = 0$) $\gamma(q_1) + \gamma^*(q_2) \rightarrow X$. The diagram of fig. 19(b) has both q_1^2, q_2^2 small but has large momentum transfer, t and leads to the large-p_T production $\gamma+\gamma \rightarrow q + \bar{q} \rightarrow$ 2 jets. This is the 2γ analogue of the single-γ jet production process $e^+e^- \rightarrow \gamma \rightarrow q + \bar{q} \rightarrow$ 2 jets seen for $Q^2 > 25$ GeV^2. The $\gamma\gamma \rightarrow$ jet + jet processes, however, can be distinguished experimentally, from $e^+e^- \rightarrow$ 2jets, since the jets in the 2γ process are not back to back and have a smaller W value. All these techniques are well known from studies at PETRA and PEP and have been successfully applied to isolate the two-photon processes being discussed.

The differential cross-section for the process $e^+e^- \rightarrow e^+e^-X$ shown in figs. (19) can be written as

$$d^2\sigma/dx\,dy\,(e^+e^- \rightarrow e^+e^-X) = 16\pi\alpha^2 E E_\gamma \times \left\{(1-y)F_2^\gamma(x,Q^2) + xy^2 F_1^\gamma(x,Q^2)\right\} f^{\gamma/e}(z)dz \quad (3.21)$$

where the variables are defined as ($E = E_{beam}$)

$$\begin{aligned} q^2 &= -Q^2 \\ x &= \frac{Q^2}{Q^2+W^2} \\ y &= 1 - \frac{E'}{E}\cos^2\theta/2 \\ z &= E_\gamma/E \end{aligned} \quad (3.22)$$

with E' and θ being the energy and scattering angle of the tagged electron. The function $f^{\gamma/e}(z)$ is the probability of finding a γ in an electron with fractional momentum z and is given by

$$f^{\gamma/e}(z) = \frac{\alpha}{\pi}\ln\left(\frac{E}{m_e}\right) + \frac{1+(1-z)^2}{z} \quad (3.23)$$

$F_{1,2}^\gamma(x,Q^2)$ are the structure functions of the photon. The longitudinal

structure function F_L is defined as

$$F_L^\gamma = F_2^\gamma - 2x F_1^\gamma \tag{3.24}$$

In a typical experiment $x\, y^2 << 1$ and so only F_2^γ is usually measured. This may, however, change at LEP, where preliminary studies have led to the hope of eventually measuring F_L^γ at LEP energies.

In the quark parton model, the diagram contributing to F_2^γ and F_L^γ is shown in fig. (20a). This gives [82]

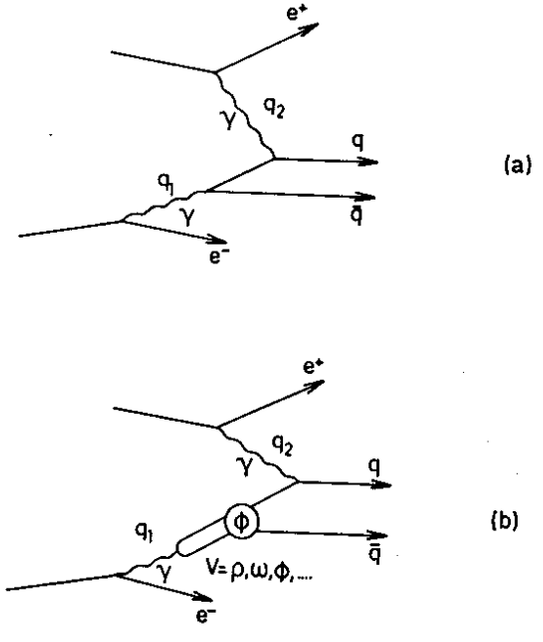

Fig. 20: Graphs contributing to the photon structure functions
a) quark parton component
b) hadronic photon component

$$F_2^\gamma(x,Q^2) = 3\sum_q e_q^4 \frac{\alpha}{\pi} x\left[x^2+(1-x)^2\right] \times \ln(Q^2/m_q^2)$$
$$F_L^\gamma(x,Q^2) = 3\sum_q e_q^4 \frac{\alpha}{\pi} 4x^2(1-x) \tag{3.25}$$

There is, however, a component in $\sigma(e^+e^- \to e^+e^-x)$ which involves hadronic wave functions in the target photon, shown in fig. (20b). Here a γ converts first into vector mesons $\gamma = V = \rho, \omega, \phi$ and then the scattering takes place between γ^* and V giving $\gamma^* V \to X$. Thus, in the vector meson dominance model, VDM, one has, for example,

$$F_2^{VDM}(x) = \alpha/(f_\rho^2/4\pi)\ \frac{1}{4}(1-x) \tag{3.26}$$

where the ρ-coupling constant has the value $f_\rho^2/4\pi \simeq 2.2$. The two contributions to the structure function $F_2^\gamma(x,Q^2)/\alpha$ are shown in fig. (21) at $Q^2 = 25\ \mathrm{GeV}^2$ with the quark model contribution from u,d and s quarks.

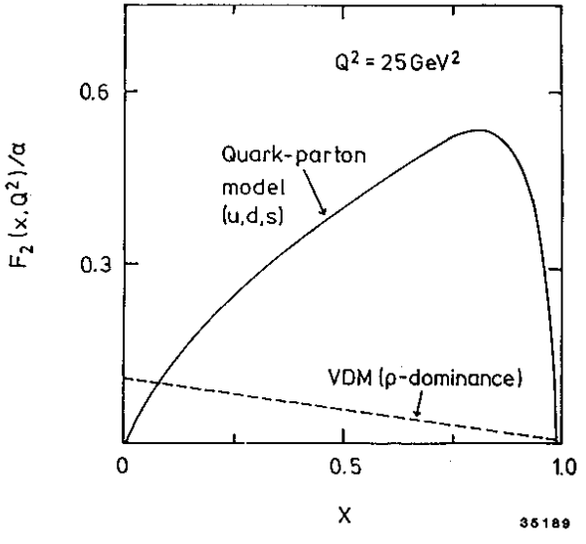

Fig. 21: The contribution to F_2^γ/α in the quark parton model and in vector dominance model

There are two more contributions that one has to include before attempting a comparison with data, namely $\gamma\gamma^* \to c\bar{c}$ and the QCD corrections. The former contributions have been calculated in ref. (83) and the latter in a number of papers [84], starting with Witten [85], who showed that QCD predicts, unlike hadron structure functions, the normalization, shape and evolution with Q^2 of the F_i^γ to second order in $\alpha_s(Q^2)$. The basic scaling behaviour, $F_2^\gamma(x,Q^2) \sim \ln(Q^2)\, f(x)$ predicted by QCD as well as the shape (x-dependence) has now been confirmed for $0.3 < x < 0.8$ by experiments at PEP and PETRA [19] for Q^2 in the range $2\ \text{GeV}^2 < Q^2 < 100\ \text{GeV}^2$. Thus, there already exist clear evidence of a large point-like contribution to F_2^γ. The question is whether the normalization can also be entirely determined by QCD. In higher order QCD calculations, the problems associated with the separation of a hadronic piece from a truely asymptotic (point-like) contribution have turned out to be somewhat intractable. There are many scenarios that exist in the literature. They range from giving up altogether the prediction of the normalization of $F_2^\gamma(x,Q^2)$ [86] and be content with the Q^2 evolution, just like the hadronic structure functions, to regularizing the singularity [87] of the second moment $M_2(x,Q^2)$ of the photon structure function by introducing a parameter thus enabling detailed QCD predictions; for $x > x_0$ ($\simeq 0.25$) there is apparently little sensitivity to the hadronic input. This latter method has recently been used by PLUTO in the analysis of F_2^γ yielding $\Lambda_{\overline{MS}} = 160 \pm 45$ MeV [88]. There are still theoretical uncertainties about the VMD background and identification of the $c\bar{c}$ component. More theoretical and experimental work is needed to settle this issue. The main point to remember is that the data suggest that the point-like contribution in F_2^γ is dominant. This implies that $F_i^\gamma(x,Q^2)$ are essentially predictable by QCD, despite setbacks for low x values.

The quality of $\gamma\gamma$ physics in terms of F_i^γ measurements is expected to be superior at LEP compared to the PEP and PETRA physics. This comes from better small angle tagging at LEP (typically $\theta(\text{min}) = 30\text{-}50$ mr compared to PETRA experiments with typical $\theta(\text{min}) \simeq 120$ mr) and continuous acceptance from this smallest angle to $\pi/2$. We show the Q^2 and W^2 distributions for typical tagging at PETRA and LEP in figs. (23). This shows the large increase in the event rates at LEP for large W^2 and Q^2 values. The average value $\langle W^2 \rangle$ is expected to be around 26-27 GeV

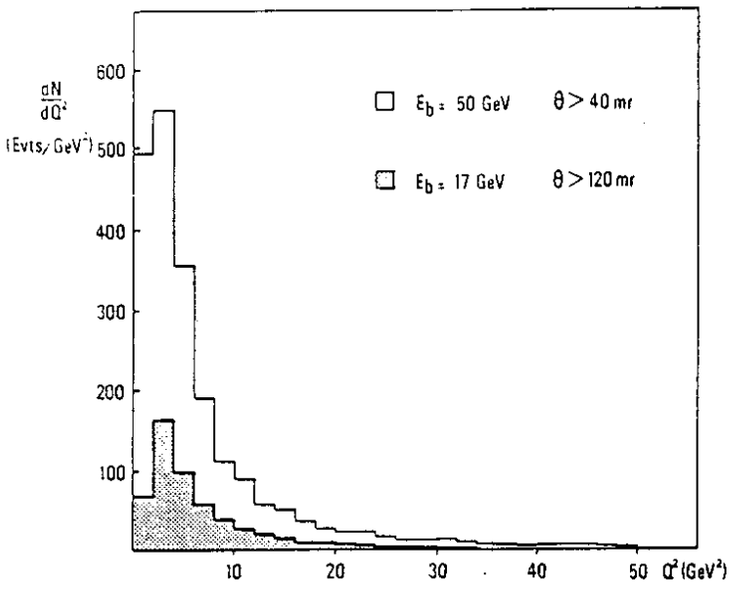

Fig. 23(a): Q^2 distribution for LEP and PETRA detector (from ref. 16)

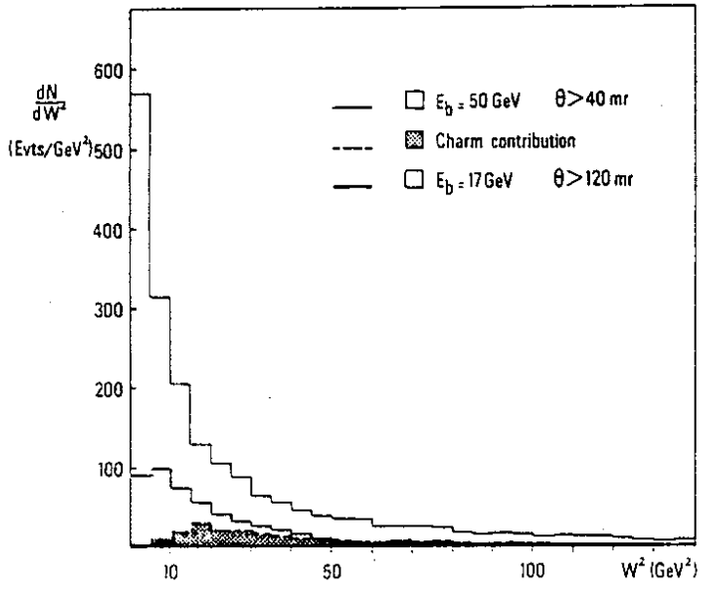

Fig. 23(b): W^2 distribution for LEP and PETRA detectors (from ref. 16)

at LEP compared to 22 GeV at PETRA. The average values $\langle Q^2 \rangle$ at PETRA and LEP are comparable since the detectors at LEP also have a better small Q^2 acceptance. For event rates at LEP and PETRA we refer to the contribution from Cordier [16].

3.4 High transverse momentum inclusive hadron production

An area of considerable theoretical and experimental activity in $\gamma\gamma$ physics is jet and hadron production at high p_T [11]. We have just discussed that the photon structure function $F_2^\gamma(Q^2)$ is dominated at large Q^2 by the pointlike couplings of the photon. For real photons (fig. 19b) it is expected that the process $\gamma\gamma \to q\bar{q}$ would show up for large transverse momenta of the quarks in large-p_T jets. For large-p_T inclusive hadron production quark-parton model predicts

$$d\sigma/dx_T\,(e^+e^- \to \gamma\gamma \to q\bar{q} \to \text{hadrons}) \sim R_{\gamma\gamma}\left(\frac{\alpha}{2\pi}\ln\left(\frac{s}{4m_e^2}\right)\right)^2 \frac{1}{x_T^4} \qquad (3.27)$$

where in the fraction quark charge model

$$R_{\gamma\gamma} = 3\sum e_q^4 = 34/27 \quad \text{for } q=u,d,s,c \qquad (3.28)$$

Experimentally, the p_T^{-4} tail is seen above $p_T > 3$ GeV, the normalization of the jet production cross-section however is higher than predicted by QCD. The inclusive-p_T distribution of hadrons dN/dp_T^2 likewise is found to be in excess of the $\gamma\gamma \to q\bar{q}$ Born term estimates [11]. Thus, it seems that for p_T^h as high as 3 GeV, the contribution of the vector meson component is not small. These experimental results have led to the speculation [89] for the quarks to be integrally charged, which we shall not entertain here.

The $O(\alpha_s)$ correction to the process $\gamma\gamma \to q\bar{q}$ giving $\gamma\gamma \to q\bar{q}g \to 3$ jets was calculated some time ago [90]. Recently the complete $O(\alpha_s)$ corrections to the process $\gamma\gamma \to q\bar{q}X \to hx$ was redone by Aurenche et al. [91], who also calculated the contribution of the hadronic component of the photon to the large-p_T $\gamma\gamma \to hx$ production process. The sum of the QCD corrected

Born term and the VDM estimate are higher than the Born cross-section by a factor 2.6 at $p_T^2 = 6$ GeV^2 and by a factor 2 at $p_T^2 = 10$ GeV^2 at PETRA energies.

Going over from PETRA ($E_{beam} = 17$ GeV) to LEP-I ($E_{beam} = 50$ GeV) to LEP-II ($E_{beam} = 100$ GeV), the QCD correction factor increases. This is shown in fig. (24). Note that the VDM contribution is still important

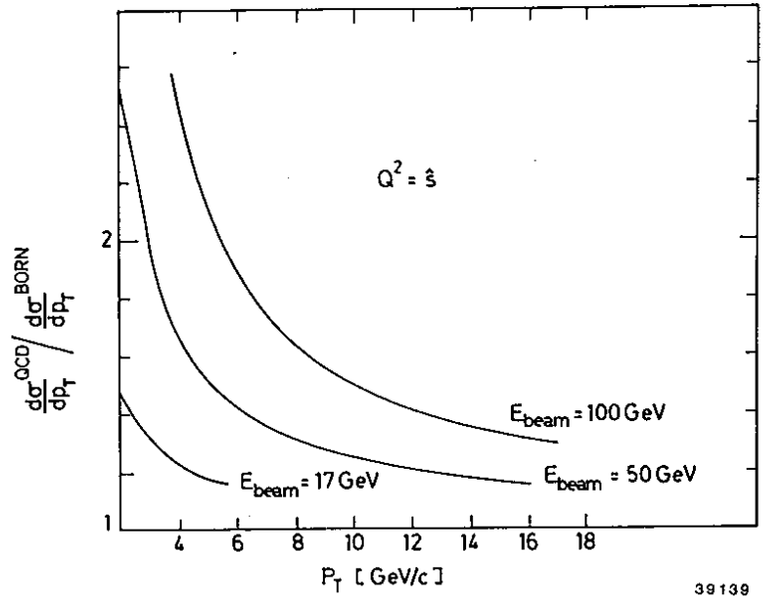

Fig. 24: The ratio of the differential spectrum calculated in QCD over the corresponding quantity calculated in the Born approximation (from ref. 17)

at LEP energies upto $p_T = 5$ GeV. , shown in fig. (25). The VDM component however has a steeper fall-off beyond $p_T = 5$ GeV and it seems that tests of QCD in $\gamma\gamma \to h+x$ will be doable only beyond $p_T = 6$ GeV. The details of the calculations are given by Aurenche et al. in a companion report. [17]

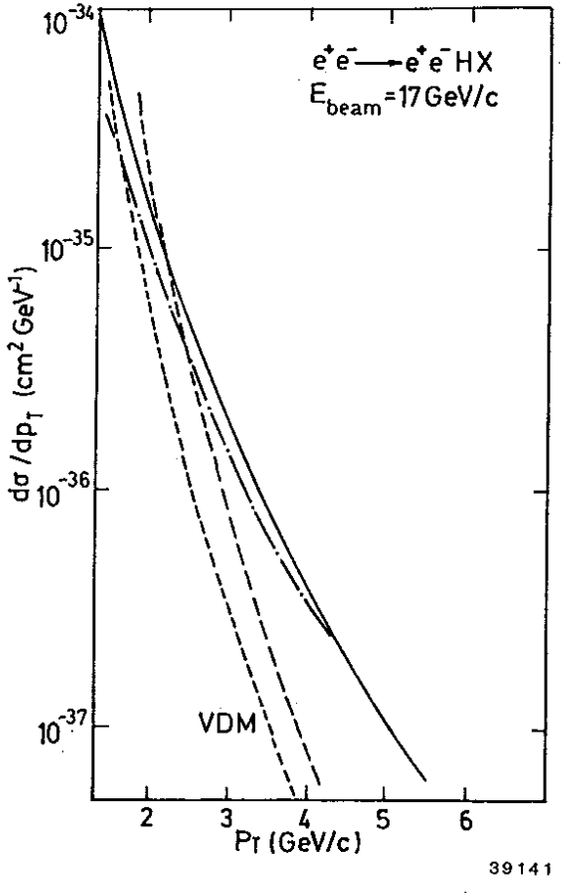

Fig. 25: The differential cross-section for the process $e^+e^- \rightarrow e^+e^-Hx$ for E_{beam} = 50 GeV. The upper QCD curve is calculated with the scale $Q^2 = p_T^2$ and the lower one with $Q^2 = \hat{s}$ = ws (from ref. 17)

3.5 Supersymmetric contributions to F_2^γ and F_L^γ

We have discussed the standard model contributions to the structure functions $F_i^\gamma(x,Q^2)$. They are dominated by the point-like contributions from the u,d,s,c quarks and QCD evolution. The bottom quark contribution is small due to the charge factor $\propto e_b^4$ and the process $\gamma\gamma \rightarrow t\bar{t}$ has kinematic suppression for large top quark masses.

The photon structure function, however, can receive contributions from new particle production. In particular, the contributions of SUSY particles to $F_i^\gamma(x,Q^2)$ have been calculated in ref. (18). The lowest order diagram contributing to $\gamma\gamma^* \rightarrow \tilde{q}\bar{\tilde{q}}$, is shown in fig. 26(a). If

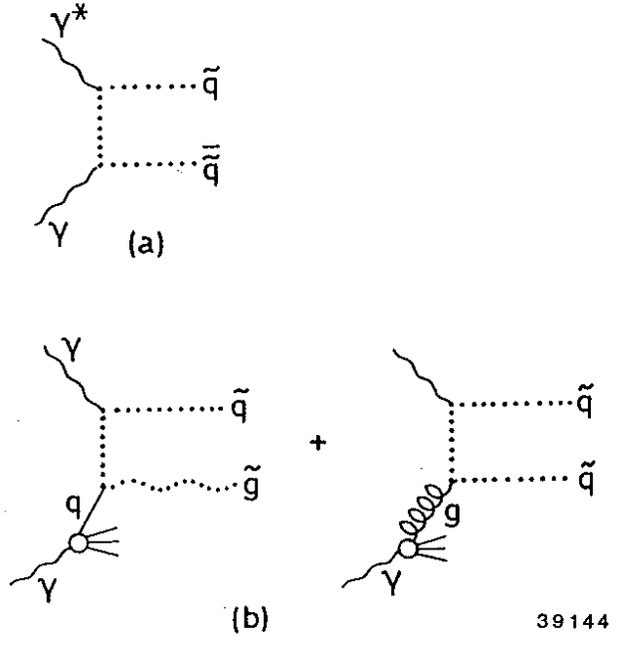

Fig. 26: SUSY particle contribution to the deep inelastic scattering

a) $\gamma\gamma^* \rightarrow \tilde{q}\bar{\tilde{q}}$
b) $\gamma\gamma^* \rightarrow \tilde{q}\tilde{g}\chi$ and higher order contribution to $\gamma\gamma^* \rightarrow \tilde{q}\bar{\tilde{q}}$

$m_{\tilde{g}} < m_{\tilde{q}}$, then the higher order diagram giving $\gamma\gamma^* \to \tilde{q}\tilde{g}\gamma$ shown in fig. 26(b) will also contribute. The second diagram of fig. 26(b) is a higher order contribution to $\gamma\gamma^* \to \tilde{q}\bar{\tilde{q}}qq$ and is very small due to the $f_{\gamma/g}$ density.

The contributions to $F_2^{\gamma}(x,Q^2)$ and $F_L^{\gamma}(x,Q^2)$ based on fig. 23(a) can be expressed as

$$\tilde{F}_L^{\gamma} = 3\sum_q e_q^4 \frac{\alpha}{\pi}(2x^2)\left\{\left[(1-x) + \tfrac{1}{2}\tau x\right] \times \ln\left(\frac{1+v}{1-v}\right) - 3v(1-x)\right\} \qquad (3.29)$$

$$\sim \ln(Q^2/m_{\tilde{q}}^2) \text{ for } Q^2 \gg m_{\tilde{q}}^2$$

$$\tilde{F}_2^{\gamma} = 3\sum_q e_q^4 \frac{\alpha}{\pi} x\left\{\left[2x(1-x) + \tau x(3x-1) + \tfrac{1}{2}\tau^2 x^2\right]\ln\left(\frac{1+v}{1-v}\right) + \left[1 - 8x(1-x) + \tau x(1-x)\right]v\right\} \qquad (3.30)$$

where

$$\tau = 4m_{\tilde{q}}^2/Q^2 \;,\quad v^2 = 1 - \tau x/(1-x) \qquad (3.31)$$

We show in fig. (27) the contribution of the SUSY interactions to the ratio $F_{L,q+\tilde{q}}^{\gamma}(Q^2)/F_{L,q}^{\gamma}(Q^2)$ as a function of τ^{-1} where $F_L^{\gamma}(Q^2)$ is defined by integrating $F_L(Q^2,x)$ over x. Thus, it is seen that for $m_{\tilde{q}} = 40$ GeV, this ratio hardly deviates from 1 upto $Q^2 = 10^4$ GeV^2. This is an astronomical value for Q^2 at LEP energies as can be seen from the (W^2,Q^2) plot in figs. (23). The contributions to F_L from the standard and SUSY sources for fixed values of x = 0.15, 0.3 are shown in fig. 28(a) as a function of Q^2. The contribution to $F_L^{\gamma}(x,Q^2)$ at $Q^2 = 10^4$ GeV^2 are shown in fig. 28(b). The contributions to $F_2^{\gamma}(x,Q^2)$ at $Q^2 = 5000$ GeV^2 and 10^4 GeV^2 are shown in fig. 29(a) and 29(b) respectively. The calculations in figs. 28 and 29 are based on $m_{\tilde{q}} = m_t = 30$ GeV and $m_{\tilde{g}} = 10$ GeV.

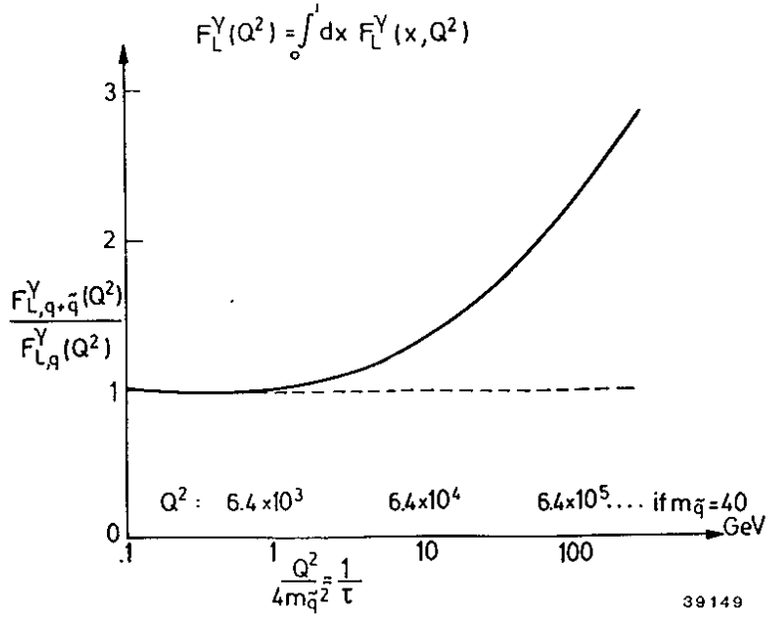

Fig. 27: SUSY contribution to the photon structure function $F_L^{\gamma}(Q^2)$ (contribution from W.J. Stirling)

From these detailed calculations it is fair to assume that the standard photon structure functions $F_2^{\gamma}(x,Q^2)$ and $F_L^{\gamma}(x,Q^2)$ will be measurable at LEP with rather high precision. However, the contributions of SUSY particles to F_i at LEP (including phase II) energies will not be detectable.

We have discussed in this section some salient features of the Photon Photon Physics at LEP energies; this survey is by no means complete. The obvious topics that are missing among others are the four-lepton processes $e^+e^- \to e^+e^-(e^+e^-,\ \mu^+\mu^-,\ \tau^+\tau^-)$ and the total cross section $\sigma^{tot}_{\gamma\gamma}(W)$. For the four lepton final states, detailed Monte Carlo programmes exist [92] which are at the disposal of our experimental colleagues. The total $\gamma\gamma$ cross-section $\sigma_{\gamma\gamma}(W)$ though huge, like its counterparts $\sigma_{pp}(\sqrt{s})$ and $\sigma_{p\bar{p}}(\sqrt{s})$, is dominated by soft hadronic processes, which we have not studied. The emphasis in this report is on

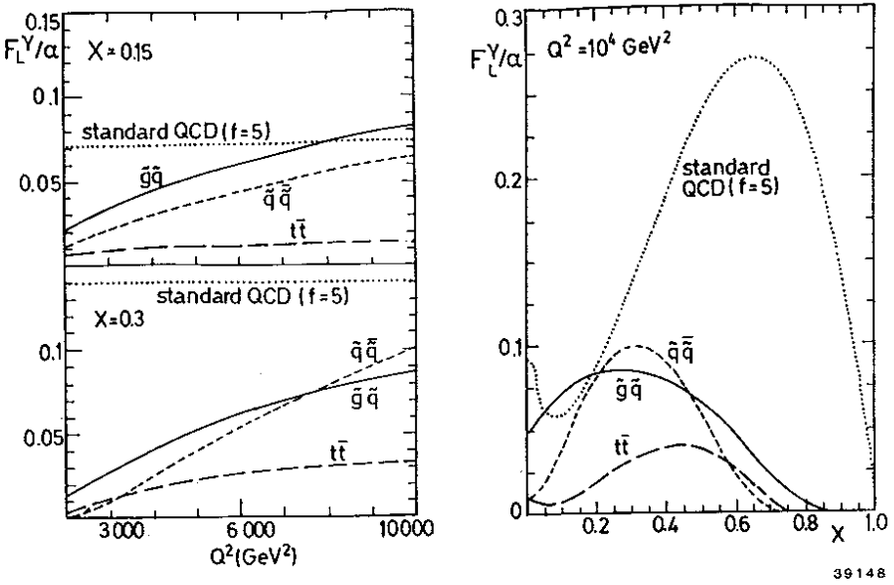

Fig. 28: Contributions of the standard (including $t\bar{t}$) and SUSY processes to F_L^γ with $m_{\tilde{q}} = m_t = 30$ GeV and $m_{\tilde{g}} = 10$ GeV (contribution from W.J. Stirling).
a) $F_L^\gamma/\alpha(x,Q^2)$ as a function of Q^2 for fixed x = 0.15 and 0.3
b) $F_L^\gamma/\alpha(x,Q^2)$ as a function of x for fixed $Q^2 = 10^4$ GeV^2

hard scattering phenomena, which are at least in principle calculable from QCD. Also left out are the parity-violating electroweak effects and Higgs production due to the "equivalent" Z^0 and $W^\pm$ beams from $e \to eZ^0$ and $e \to \nu W$. Strictly speaking, they do not belong to the $\gamma\gamma$ domain and we hope that they have been considered by others elsewhere.

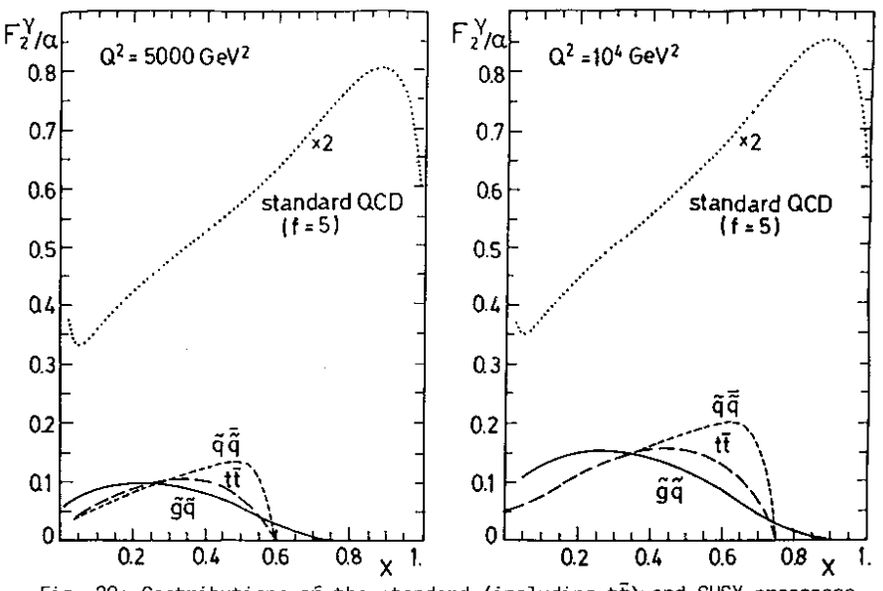

Fig. 29: Contributions of the standard (including $t\bar{t}$) and SUSY processes to F_2^γ with $m_{\tilde{q}} = m_t = 30$ GeV and $m_{\tilde{g}} = 10$ GeV (contribution from W.J. Stirling)
a) $F_2^\gamma/\alpha(x,Q^2)$ as a function of x at $Q^2 = 5000$ GeV^2
b) Same as (a) with $Q^2 = 10^4$ GeV^2

4. Heavy quark physics at LEP

We briefly recapitulate here the work done on studies of heavy quark production and decay properties at LEP. The two topics on which we have concentrated are the bottom and top quark physics.

The decay width of the top quark is expected to be large due to the $\Gamma(t) \sim m_t^5$ dependence and the CKM matrix element $V_{tb} \sim 1$. The width $\Gamma(t)$, calculated upto $O(\alpha_s)$ QCD corrections, is shown in fig. (30). The impact of large $\Gamma(t)$ on the decay pattern of toponium bound states is discussed by the study group on toponium physics at LEP [29].

The decays $Z^0 \to t\bar{t}$, if allowed kinematically, will yield top quarks with a high degree of polarization. Since the M1 transitions in the decays of the vector top meson, T*, will be overwhelmed by the single

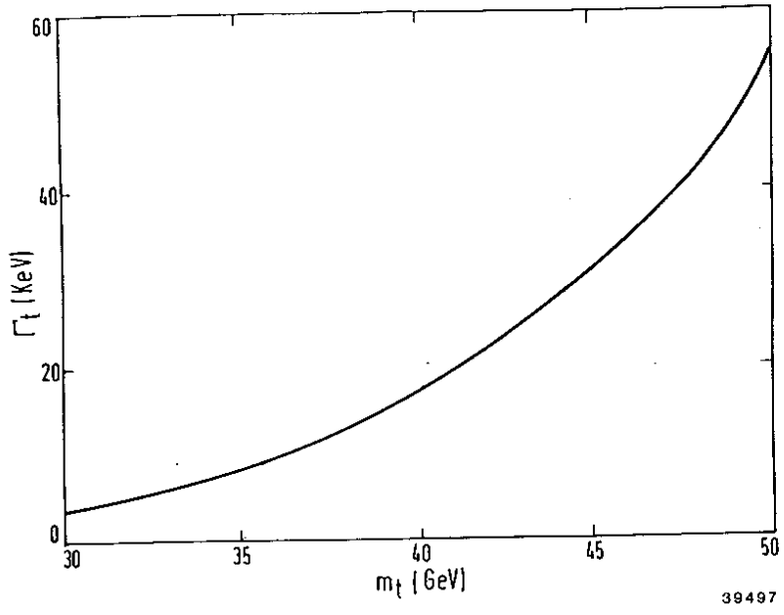

Fig. 30: Top quark decay width as a function of m_t (from ref. 24)

quark decay, SQD, mechanism, also T* will decay weakly. One expects measurable effects of the top quark polarization on the production (i.e. fragmentation) and decay distributions. In particular, the effects on the forward-backward charge asymmetry for exclusive channels $e^+e^- \rightarrow T\bar{T}$, $T\bar{T}^*$ etc. will be important. The inclusive charge asymmetry for $e^+e^- \rightarrow t\bar{t} \rightarrow l^-x$ is also expected to be significantly effected, more so if m_t is large $\gtrsim$ 40 GeV. Top quark polarization have measurable effects on the decay distribution from $t \rightarrow l^-x$, in particular the lepton energy distribution is sensitive to the depolarization parameter, and has some bearings on the issue of m_t determination as well as on attempts to determine the CKM ratio V_{ts}/V_{tb} from semileptonic decays of the top quark. All these points are discussed in detail in ref. (24).

The other topic that we have studied at quite some length concerns the bottom quark production and decay properties. Bottom physics is

a rapidly progressing field, thanks to experiments at CESR, DORIS, PEP, PETRA and CERN. The impressive measurements of the average bottom lifetime, $\langle \tau_B \rangle$, semileptonic branching ratios, stringent limits on the ratio $|V_{bu}/V_{bc}|$ enabling determination of the matrix element $|V_{bc}|$, and hints from the collider on the presence of B-$\bar{B}$ oscillations are the present highlights of the bottom physics. Probably, the most important questions in bottom decays at the time of LEP turnon would be the determination of the matrix element $|V_{bu}|$, confirmation of the B-$\bar{B}$ oscillations, measurements of the individual bottom hadron lifetimes and exclusive branching ratios, and certainly the issue of CP violations in bottom sector. We have addressed each of these questions in ref. (24).

The figure of merit for experiments in bottom physics is the efficiency in reconstructing specific bottom mesons. An estimate of the efficiency of charmed and bottom hadron detection at LEP is shown in fig. 31. (25) The degree of success of the experimental programme at LEP in studies of heavy quark physics depends largely on the resolution and efficiency of the vertex detectors.

The transverse momentum distribution of the charged lepton, dN/dp_T^l, in the semileptonic decays of heavy quarks is sensitive to the ratio (m_Q/m_q) and hence can be used to distinguish the decays $b \rightarrow c l \nu_l$ from $b \rightarrow u l \nu_l$ as shown in fig. 32. The large bottom hadron statistics from the decays $Z^0 \rightarrow b\bar{b}$ would make LEP experiments competitive with the experiments at CESR and DORIS.

The experiments at LEP are particularly suited to study B-$\bar{B}$ oscillations. This can be done using one or all of the following measurements
(i) Measuring the ratio $R(^{++}_{--}/+-)$ in the inclusive dilepton final state in the process $e^+e^- \rightarrow b\bar{b} \rightarrow l^+l^+x, l^-l^-x$. The expected ratio $R(B_s)$ and $R(B_d)$ from the processes

$$e^+e^- \rightarrow B_d^0 X \rightarrow llX$$
$$\rightarrow B_s^0 X \rightarrow llX \qquad (4.1)$$

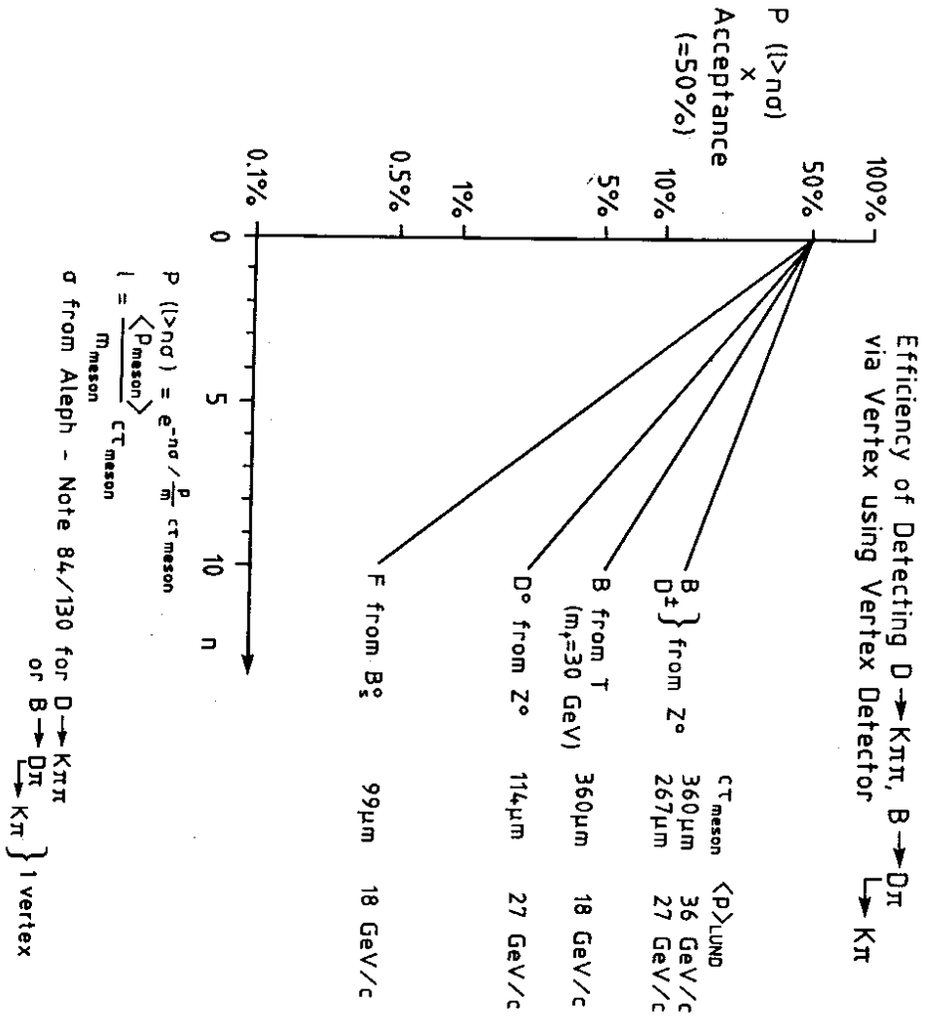

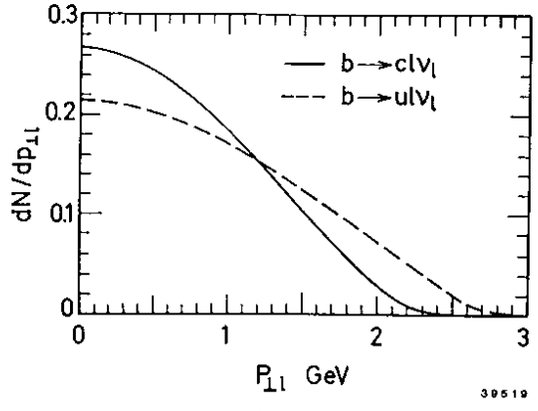

Fig. 32: Transverse lepton energy distributions in the semileptonic decays measured with respect to the bottom quark (= jet) axis in $e^+e^- \to b\bar{b} \to l^- x$. The relative normalization of dN/dp_T^l ($b \to u/b \to c$) is given by the ratio $R \equiv \Gamma(b \to u l \nu_l)/\Gamma(b \to c l \nu_l)$ (from ref. 24).

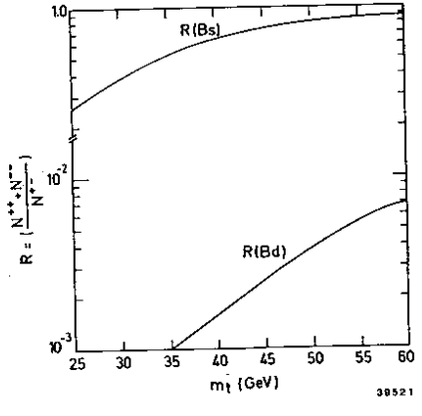

Fig. 33: The same sign to opposite sign dilepton ratio in the process $e^+e^- \to B_s^0 X \to llX$ and $e^+e^- \to B_d^0 X \to llX$ (from ref. 24).

are shown in fig. (33) as a function to top quark mass. The expected ratio of $R(^{++}_{--}/+-) \simeq 0.15$.

(ii) The difference in the forward-backward charge asymmetry A^b_{FB} in the process $e^+e^- \to b\bar{b}x$. Denoting by A_{FB} the standard value and by $\bar{A}_{FB}$ the measured value one can show that

$$\frac{\bar{A}^b_{FB}(e^+e^- \to b\bar{b} \to \ell^\pm x)}{A^b_{FB}} \simeq (1-2\chi) \qquad (4.2)$$

one expects $\bar{A}^b_{FB}/A^b_{FB}$ 0.85 with complete mixing in the B_s-$\bar{B}_s$ sector.

(iii) Measuring the lepton-kaon-kaon asymmetry

$$\Delta R(\ell KK) \equiv \frac{[\sigma(\ell^\mp K^\mp K^\mp_X) - \sigma(\ell^\mp K^\pm K^\pm_X)]}{[\sigma(\ell^\mp K^\mp K^\pm_X) + \sigma(\ell^\mp K^\pm K^\pm X)]}$$

in the process $e^+e^- \to b\bar{b} \to$ lKKX. The dependence of ΔR(lKK) and $R(^{++}_{--}/(++)+(--)+(+-))$ are shown in figs. (34) as a function of χ, the B-$\bar{B}$ mixing measure.

It seems to us that the prospects of measuring the B-$\bar{B}$ oscillations at the level $\chi \gtrsim 0.04$, expected in the standard model are quite bright.

Finally, we have discussed the problem of CP violation measurements at LEP through the asymmetry $a = (N_{++} - N_{--})/(N_{++} + N_{--})$ in the dileptons and in a number of exclusive bottom hadron decays. The intrinsic strength of CP-violation, though in some specific partial decays not small, would still require $O(10^7$-$10^8)$ bottom hadrons. Reconstruction of bottom hadrons in interesting decay channels will help, though in almost all cases these channels are either suppressed in the CKM sense or lead to multi-particle states. The intrinsic rate for the charge asymmetry a in the standard model is rather small, $O(10^{-4})$. This, however, may change in a number of non-standard scenarios. In any case, experiments at LEP provide a good laboratory to study CP violation in bottom hadron sector.

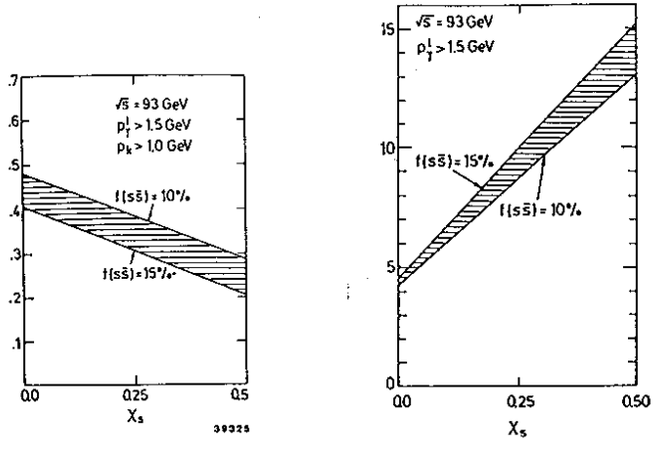

(a) (b)

Fig. 34: The ratio (a) ΔR(lKK) and (b) R(ll) as functions of the mixing measure χ_s with the indicated values of the parameters in e^+e^- annihilation. Here R(ll) = (N++ + N−−)/(N++ + N−− + N+−).

5. Summary and conclusions

Physics at LEP is certainly going to be very exciting! Quite apart from the high discovery potential of LEP for observing physical phenomena outside of the standard model, LEP provides an intense and energetic source of quarks, gluons, leptons, Z^0 bosons and photons. Thus, it is an excellent laboratory to undertake precision studies in the standard theory of electroweak interactions and QCD.

Jets in e^+e^- are by far the cleanest. The large energy as well the very high rates for $Z^0 \to$ 2,3-,4-,... jets well separated from each other will allow to do a much detailed quantitative test of QCD. Confirmation of the non-abelian nature of QCD, precise determination of $\alpha_s(Q^2)$, determination of the electroweak coupling constants of quarks and leptons, through measurements of R, Γ_Z and asymmetries belong to the main area of experimental activity at LEP.

The quality of photon photon physics at LEP is expected to be lot better than at lower existing e^+e^- facilities due to the larger W^2, Q^2 regions that would be available at LEP. Moreover , small angle tags will increase the counting rates. We find that experiments at LEP will enable precision measurements of the photon structure function, F_i^γ. The dependence of $F_2^\gamma(Q^2) \sim 1/\alpha_s(Q^2) \sim \ln(Q^2/\Lambda^2)$, which though already discernible at PEP and PETRA, will become more pronounced. In addition, first measurements of the longitudinal structure function, $F_L^\gamma(Q^2)$, will be possible at LEP. In addition, measurements of jets in $\gamma\gamma \to q\bar{q}$, large-$p_T$ production of inclusive hadrons, production of gluonic and multiquark states, large Q^2 production of hadrons in exclusive processes would provide new testing grounds for QCD.

The main interest in LEP Physics, however, lies in its capability of measuring rare and new processes. There are three rare processes which are of main interest in the weak decays of bottom quark, namely, measurements of the CKM suppressed transition $b \to u$, the phenomena of B-$\bar{B}$ oscillations and CP violation. We are optimistic about the measurements of the first two processes at LEP; measurements of CP violations at LEP, however, most probably would signal the presence of non-standard sources of CP violation and hence will constitute a breakthrough.

Last but not least, LEP and SLC could become probably the only machines with intense top quark beams produced in background free environment. This would be an entirely new area of physics. The least that LEP is capable to do is test the hypothesis that the top quark belongs to a regular SU(2) doublet with canonical properties and couplings. The large top quark mass may, however, trigger new physics that very probably we have not thought about. That would be the real bonus of LEP!

Acknowledgements

I have enjoyed enormously working with my colleagues in the study group on QCD, $\gamma\gamma$ and heavy quark physics at LEP and I would like to warmly thank them for their support and many discussions. Contributions of B. Adeva and R. Barlow are also acknowledged. I am grateful to my colleagues at DESY and the University of Hamburg for discussions and help in the preparation of this manuscript, especially G. Ingelman, B. Lampe, G. Kramer, B. Naroska and G. Nowak. Last but not least the help of Frau H. Laudien in typing the manuscript and of Frau H. Evers and Herrn Knaut in drawing the numerous figures is gratefully acknowledged.

Appendix A

The fully differential distributions in the process $e^+e^- \to q\bar{q}g$. The "parity-even" part of the cross-section (involving VV and AA couplings in the lepton and quark-gluon sector) has the decomposition:

$$\frac{d\sigma}{dx_q\,dx_{\bar{q}}\,d\cos\theta\,d\chi/2\pi} = \frac{3}{8}(1+\cos^2\theta)\frac{d\sigma^U}{dx_q dx_{\bar{q}}} + \frac{3}{4}\sin^2\theta\frac{d\sigma^L}{dx_q dx_{\bar{q}}} - \frac{3}{2\sqrt{2}}\sin 2\theta\cos\chi\frac{d\sigma^I}{dx_q dx_{\bar{q}}} + \frac{3}{4}\sin^2\theta\cos 2\chi\frac{d\sigma^T}{dx_q dx_{\bar{q}}}$$

and the "parity-odd part" (i.e. parity-odd V-A current products in the lepton sector as well as in the quark-gluon sector) has the decomposition

$$\frac{d\sigma}{dx_q\,dx_{\bar{q}}\,d\cos\theta\,d\chi/2\pi} = \frac{3}{4}\cos\theta\frac{d\sigma^F}{dx_q dx_{\bar{q}}} - \frac{3}{2\sqrt{2}}\sin\theta\cos\chi\frac{d\sigma^X}{dx_q dx_{\bar{q}}}$$

$x_q = 2E_q/\sqrt{s}$ denotes the scaled energy of the outgoing quark, etc. (from energy conservation, $x_q + x_{\bar{q}} + x_G = 2$); the angles θ and χ are shown in Fig. 1. The various parts of the cross section correspond to the following combination of (γ,Z) helicities, the quantization axis chosen along the momentum defining the angle :

U = unpolarized transverse
L = longitudinally polarized
I,X = longitudinal/transverse interference
T = +/- interference
F = difference between right/left polarization

References

1. For a recent survey see, for example, F. Barreiro, DESY Report DESY 85-008 (1985); G. Altarelli, Proceedings of the EPS Conference on High Energy Physics, Bari, Italy (1985) and Univ. of Rome Preprint No. 477 (1985).

2. See, for example, D.H. Saxon, Rutherford Lab. Report RAL-85-077 (1985).

3. G. Sterman and S. Weinberg, Phys. Rev. Lett. 39, 1436 (1977).

4. J. Ellis, M.K. Gaillard and G.G. Ross, Nucl. Phys. B111, 253 (1976).

5. D.P. Barber et al. (MARK J Collaboration), Phys. Rev. Lett. 43, 830 (1979);
Ch. Berger et al. (PLUTO Collaboration), Phys. Lett. 86B, 418 (1979);
R. Brandelik et al. (TASSO Collaboration), Phys. Lett. 86B, 243 (1979).

6. J. Ellis and I. Karliner, Nucl. Phys. B148, 141 (1979); For an experimental survey see, for example, S.L. Wu, Phys. Reports 107C, No. 2-5 (1984).

7. R.K. Ellis, D.A. Ross and E.A. Terrano, Nucl. Phys. B178, 421 (1981); J.A.M. Vermaseren, K.J.F. Gaemers, S.J. Oldham, Nucl. Phys. B187, 301 (1981); K. Fabricius, G. Kramer, G. Schierholz, I. Schmitt, Z. f. Phys. C11, 315 (1982).

8. For a recent survey of $\alpha_s(Q^2)$ determinations see R.Y. Zhu, Proceedings of the APS Meeting, Santa Fe (1985). See also ref. (1).

9. See for example A. Silverman, Proceedings of the XXII International Conference on High Energy Physics, Leipzig, DDR (1984).

10. For experimental and theoretical surveys of Υ system see, respectively, P.M. Tuts and G.P. Lepage, Proc. of the 1983 Int. Symp. on Lepton and Photon Interactions at High Energies, Cornell, Ithaca (1983).

11. For an experimental update on $\gamma\gamma$ collisions see, for example, H. Kolanoski, Proceedings of the 1985 International Symposium on Lepton and Photon Interactions at High Energies.

12. PLUTO Coll., Ch. Berger et al., Phys. Lett. 142B (1984) 125;
CELLO Coll., H.-J. Behrend et al., Phys. Lett. 126B (1983) 391;
JADE Coll., W. Bartel et al., Phys. Lett. 121B (1983) 203; Z. Phys. C24 (1984) 231;
TPC/$\gamma\gamma$ Coll., W. Wagner, Proc. of the $\gamma\gamma$ Workshop, Lake Tahoe (1984);
TASSO Coll., E. Duchovni, Proc. of the $\gamma\gamma$ Workshop, Lake Tahoe (1984);
MAC Coll., E. Fernandez, Proc. of the $\gamma\gamma$ Workshop, Lake Tahoe (1984).

13. G. Rudolph, these proceedings.

14. K.H. Streng, these proceedings.

15. M. Davier, Proceedings of the Fourth International Colloquium on Photon Photon Interactions, Paris, Ed. G.W. London, World Scientific Singapore 411-436 (1981);
J.H. Field, Proceedings of the International Workshop on $\gamma\gamma$ Collisions, Amiens, Lecture Notes in Physics, Vol. 134, Ed. G. Cochard and P. Kessler, Springer-Verlag Heidelberg (1980).

16. A. Cordier, these proceedings.

17. P. Aurenche et al., these proceedings.

18. D.M. Scott and W.J. Stirling, Phys. Rev. D29, 157 (1984);
M. Glück and E. Reya, Phys. Rev. D28, 2749 (1983) and DO-TH-84/12 (1984).

19. For the present experimental status of the $\not{p}_T$-events at the collider see C. Rubbia, talk presented at the 1985 International Symposium on Lepton and Photon Interactions at High Energies, Kyoto, Japan (1985).

20. J. Ellis, M.K. Gaillard, D. Nanopoulos, Nucl. Phys. B106, 292 (1976).

21. M. Chanowitz, Proc. of the $\gamma\gamma$ Workshop, Lake Tahoe (1984).

22. J. Ellis and J. Lánik, Phys. Lett. 150B (1985) 289.

23. F. Schrempp, DESY Report, DESY 06/85 (1985).

24. A. Ali, these proceedings.

25. R. Settles, these proceedings.

26. Indirect evidence of the bottom quark belonging to a doublet is rather strong from CESR and DORIS data.

27. N. Anselmino, P. Kroll and B. Pire, Zeit. f. Physik C29, 135 (1985) CERN Report, CERN-TH-4172/85 (1985);
J.H. Kühn, A. Reither and P.M. Zerwas, SLAC PUB-3746 (1985).

28. A. De Rujula and H. Georgi, Phys. Rev. D13, 1296 (1976).

29. "Toponium Physics at LEP", W. Buchmüller et al., these proceedings.

30. M. Dine and J. Sapirstein, Phys. Rev. Lett. 43, 668 (1979);
K.G. Chetyrkin, A.L. Kataev and F.V. Tkachov, Phys. Lett. 85B, 277 (1979); W. Celmaster and R.J. Gonsalves, Phys. Rev. Lett. 44, 560 (1980).

31. W.A. Bardeen, A.J. Buras, D.W. Duke and T. Muta, Phys. Rev. D18, 3998 (1978).

32. M.A. Shifman, A.I. Vainshtein and V.I. Zakharov, Nucl. Phys. B147, 385, 448, 519 (1979).

33. See D.W. Duke and R.G. Roberts, Phys. Rep. 120, 275 (1985) and references therein.

34. R. Kleiss, these proceedings.

35. A. McDonald, R. Budny, Phys. Lett. 48B, 423 (1974).

36. B. Naroska, DESY Report 85-090 (1985) and proceedings of the meeting: "Physics in Collisions V", Autun, France (1985).

37. B. Adeva et al. MARK-J Collaboration), Phys. Rep. 109, 181 (1984); W. Bartel et al. (JADE Collaboration) in ref.85; M. Althoff et al. TASSO Collaboration), Zeit. f. Phys. C22, 219 (1984).

38. This is a consequence of parity conservation in strong interaction.

39. A. Ali, J.G. Körner, Z. Kunszt, J. Willrodt, G. Kramer, G. Schierholz, and E. Pietarinen, Phys. Lett. 82B, 285 (1979); Nucl. Phys. B167, 454 (1980).

40. See, for example ref. (2) and Wu in ref. 6.

41. E. Farhi, Phys. Rev. Lett. 39 (1977) 1587; S. Brandt et al., Phys. Lett. 12 (1964) 57.

42. A. De Rujula, J. Ellis, E.G. Floratos, M.K. Gaillard, Nucl. Phys. B138, 387 (1978).

43. See, for example, G. Kramer, DESY Report DESY 83/068 (1983).

44. E. Laermann, K.H. Streng and P.M. Zerwas, Zeit. f. Phys. C3, 289 (1980).

45. B. Lampe and G. Kramer, Commun. Math. Phys. 97, 257 (1985). DESY Report DESY 85/030 (1985); J.G. Körner, G. Schuler, G. Kramer and B. Lampe, DESY Report DESY 85-143 (1985).

46. L. Clavelli and G. v. Gehlen, Phys. Rev. D27, 1495 (1983).

47. N.H. Avram and D.H. Schiller,Nucl. Phys. B70, 272 (1974).

48. H. Goldstein, Classical Mechanics (Addison-Wesley, Reading, Mass. and London, 1959).

49. See, for example, M. Chen, Proc. of the International School of Subnuclear Physics, Erice, Italy (1985).

50. P. Binetruy, G. Girardi, Phys. Lett. 83B, 382 (1979); B.G. Weeks, Phys. Lett. 81B, 377 (1979).

51. G. Kramer, DESY-Report DESY 82-079 (1982), and Proceedings of the XIII. Spring Symposium on High Energy Physics (Karl-Marx-Univ., Leipzig) (1982).

52. T. Kinoshita, J. Math. Phys. 3, 650 (1960); T.D. Lee, M. Nauenberg, Phys. Rev. 133, 1594 (1960).

53. Lampe and Kramer in ref. 45.

54. T.D. Gottschalk, M.P. Schatz, Phys. Lett. 150B, 451 (1985); Z. Kunszt, Phys. Lett. 99B, 429 (1981) and Phys. Lett. 107B, 123 (1981); A. Ali, Phys. Lett. 110B, 67 (1982).

55. A. Ali et al., Phys. Lett. 82B (1979) 285 and Nucl. Phys. B167 (1980) 454; K.J.F. Gaemers and J.A.M. Vermaseren, Z. Phys. C7 (1980) 81.

56. One such program is called QCDJETS available at DESY. This is an updated version of the socalled Ali et al. model; A. Ali, G. Kramer, E. Pietarinen, J. Willrodt, Phys. Lett. 93B, 155 (1980).

57. C.L. Basham, L.S. Brown, S.D. Ellis, S.T. Love, Phys. Rev. D17, 2298 (1978), Phys. Rev. Lett. 41, 1585 (1978).

58. A. Ali, F. Barreiro, Phys. Lett. 118B, 155 (1982); Nucl. Phys. B236, 269 (1984).

59. D.G. Richards, W.J. Stirling and S.D. Ellis, Phys. Lett. 119B (1982) 193; Nucl. Phys. B229 (1983) 317.

60. B. Adeva et al. (MARK J Collaboration), Phys. Rev. Lett. 50, 2051 (1983); 54, 1750 (1985); M. Althoff et al. (TASSO Collaboration), Zeit. f. Phys. C6, 157 (1984); Ch. Berger et al. (PLUTO Collaboration), DESY Report 85-039 (1985).

61. J.C. Collins and D.E. Soper, Nucl. Phys. B193 (1981) 381; B197 (1982) 446.

62. B.R. Webber, Nucl. Phys. B238, 492 (1984); G. Marchesini, B.R. Webber, Nucl. Phys. B238, 1 (1984).

63. A.H. Mueller, Nucl. Phys. B213, 85 (1983); B228, 357 (1983); A. Bassetto, M. Ciafaloni, G. Marchesini, Phys. Rep. 100, 201 (1983); L.V. Gribov, E.M. Levin, M.G. Ryskin, Phys. Rep. 100, 1 (1983); Ya.I. Azimov, Yu.L. Dokshitzer, V.A. Khoze, S.I. Troyan (as quoted by Altarelli in ref. 1.

64. G.C. Fox, S. Wolfram, Z. Phys. C4, 237 (1980).

65. This certainly is not the only QED type theory that one can construct but appears to us not to be in conflict with the normalization of 2 and 3 jet cross-sections.

66. J.G. Körner, G. Schierholz, J. Willrodt, Nucl. Phys. B185, 365 (1981).

67. O. Nachtmann, A. Reiter, Z. Phys. C - Particles and Fields 16, 45 (1982).

68. J.H. Field, University of Paris Report L.P.N.H.E. 84-04 (1984).

69. H. Kolanoski, Springer Tracts in Mod. Phys., Vol. 105 (1984).

70. P.V. Landshoff and J.H. Field in Proceedings of the LEP Summer Study, CERN Report 79-01 (1979), vol. 2; see also ref. 15.

71. J.H. Field, Nucl. Phys. B168, 477 (1980) and Erratum B176, 545 (1980).

72. C.F. v. Weizsäcker, Z. Phys. 88, 612 (1934);
E.J. Williams, Proc. Roy. Soc. A139, 163 (1933);
Phys. Rev. 45, 729 (1934);
Mat. Fys. Moddelingen 13 4 (1935).

73. D. Duke and J. Owens, Phys. Rev. D30, 49 (1984) and Erratum.

74. See, for example, S. Komamiya, Proceedings of the Int. Symp. on Lept. and Phot. Interactions, Kyoto (1985)

75. M.K. Gaillard, L. Hall and I. Hinchliffe, Phys. Lett. 116B, 279 (1982).

76. See, for example, S. Dawson, E. Eichten and C. Quigg, Fermilab-Pub-83/82-THY (1983) and references therein.

77. H. Baer et al., these proceedings.

78. F.E. Low, Phys. Rev. 120, 582 (1960).

79. See, for example, A. Ali, DESY Report DESY 81-060 (1981).

80. A. Ali and M.A.B. Bêg, Phys. Lett. 103B, 376 (1981).

81. For a recent review and references see S.J. Brodsky, SLAC Report SLAC-PUB-3547 (1985).

82. C.T. Hill and G.G. Ross, Nucl. Phys. B148 (1979) 373.

83. T. Uematsu and T.F. Walsh, Phys. Lett. 101B (1981) 263;
Nucl. Phys. B199 (1982) 93.

84. W.A. Bardeen and A.J. Buras, Phys. Rev. D20 (1979) 166; Err. D21 (1980) 2041;
D.W. Duke and J.F. Owens, Phys. Rev. D22 (1980) 2280.

85. E. Witten, Nucl. Phys. B210 (1977) 189.

86. M. Glück, K. Grassie and E. Reya, Phys. Rev. D30 (1984) 1447.

87. I. Antoniadis and G. Grunberg, Nucl. Phys. B213 (1983) 445.

88. See Ch. Berger et al. (PLUTO Collaboration) in ref. 12.

89. R.M. Godbole et al., Phys. Lett. 142B (1984) 91.

90. F.A. Berends, R. Gastmans and Z. Kunszt, Nucl. Phys. B182 (1981) 397.

91. P. Aurenche et al., Annecy-Report LAPP-TH-134 (1985).

92. J.A.M. Vermaseren, Proceedings of the International Workshop on Collisions, Amiens, Lecture Notes in Physics, Vo. 134, Ed. C. Cochard and P. Kessler, Springer-Verlag Heidelberg (1980) 35-46.